FINAL REPORT

Microwave Plasma Continuous Emissions Monitor (MP-CEM)

Paul Woskov, (PI)

Plasma Science and Fusion Center
Massachusetts Institute of Technology
Cambridge, MA 02139

December 2000

Award Number: DE-FG07-98ID13601

Table of Contents

1. Stack Mountable Microwave Plasma for Sensitive Real Time Calibrated Metals and Particulate Monitoring

Paul P. Woskov, Kamal Hadidi, Karyn Green, Paul Thomas

Plasma Science and Fusion Center, Massachusetts Institute of Technology, 167 Albany Street, Cambridge, MA 02139

1.1 Abstract

A compact microwave plasma device that can be attached to a stack for near *in situ* atomic emission spectroscopy, with a real-time span calibration injector for accuracy, is under development for continuous metals monitoring. It uses a commercially available 2.45 GHz, 1.5 kW microwave source to generate a plasma in an undiluted, isokinetic flowing slipstream. The plasma is efficiently (> 98% microwave to plasma coupling) sustained in a shorted waveguide, which together with a short sample line is maintained at high temperature (> 150 °C) to avoid condensation. Relative to other plasma based CEMs the microwave plasma has a significant advantage to continuously operate reliably in large volumes (~ 50 cm^3) of fast flowing (≥ 14 l/minute, up to 40 ft/sec) air or undiluted stack exhaust. A pneumatic nebulizer attached to the sample line can momentarily, on command, inject a known trace concentration of metals to provide a real-time span calibration whenever needed. Novel grating spectrometers using low cost detectors have been used for simultaneous multiple metals monitoring with continuous rapid signal acquisition (≤ 0.20 s) making possible the observation of discreet particles. Since the particles are observed as plasma induced sources of light, the usual limits on monitoring discreet submicron particles by conventional external light instruments are not encountered. Detection limits for Be, Cr, and Pb of < 3 $\mu g/m^3$ have been shown for one minute signal averaging in plasmas with 6% water content. A one minute detection limit for Hg of ≤ 1 $\mu g/m^3$ has been recently achieved in ambient laboratory air plasmas using a dedicated spectrometer. Lower detection limits are possible with longer signal integration time. Past testing on an EPA research incinerator demonstrated the capability for monitoring metal concentrations with a relative accuracy of 20% to EPA method 29.

1.2 Introduction

There is a continuing need for better and more affordable air emissions monitoring technologies for the U. S. Environmental Protection Agency (EPA) Toxic Release Inventory (TRI) of hazardous chemicals and fine particulates. Such technologies are needed for research to better understand the environmental and health threat from various emission sources, for control of operations that produce TRI emissions, and ultimately for compliance with regulations. At present there is no single emissions monitoring technology that can observe the entire TRI list of chemicals along with the particulate size distributions, which are important for understanding pollution processes and for determining respiratory deposition and dose. In this report we focus on a microwave plasma technology that has the potential to accurately monitor only the TRI metals along

with aerosol particle size distributions down to sizes that usually cannot be discretely observed in flowing gas by conventional particle monitors.

Atomic emission spectroscopy of a plasma generated in stack exhaust or in an isokinetically extracted sample is a leading approach for real-time metals emissions monitoring. Among the various methods being used to generate a plasma for this application the microwave plasma torch has shown considerable promise. In a maiden field test attached to an EPA research incinerator stack its potential for compliance monitoring was readily demonstrated by achieving desirable sensitivity (< 3 $\mu g/m^3$) and accuracy (~ 20%) goals for a limited subset of the TRI metals for which it was instrumented (Be, Cr, and Pb) [1,2]. In earlier tests the microwave plasma device was fabricated from refractory materials and its potential as a control monitor was demonstrated by operating continuously **inside** a stack upstream of the scrubbers at temperatures > 650 °C and dense particle loading[3]. Recent laboratory development has focused on understanding the plasma mechanisms that limit *in situ* plasma detection sensitivity on some metals such as mercury [4,5].

Characterization of particle size distributions along with discreet particle chemical composition has been accomplished in the past in aerosol particulate research with laser instruments. Multiple laser beams have been used to first measure size with low power scattering and then determine chemistry with a high power pulse to volatilize the particle for either atomic emission spectroscopy[6] or analysis in a mass spectrometer[7]. However, when the particle size is less than the wavelength of light, in the Rayleigh range, the scattered light scales as $\sim r^6/\lambda^4$ and small particle become difficult to observe.

More recently Hahn[8] has shown that a laser to illuminate the particle for size measurements is not necessary. The light emission from the high power laser spark can be calibrated to determine size under the assumption that only one particle is present per pulse. Furthermore, since an external source of light is not needed, the measured light signal is not constrained by the Rayleigh limit and smaller submicron particles can be studied. In another work Takahara et al[9], have shown that light pulses due to particle transit into a continuous microwave plasma sustained in a resonator, in helium gas can also be calibrated to determine size. The light signal scaled as the particle size cubed, as expected for a signal dependent on the volatilized volume of a particle.

In this report we will show that total metals concentration and particle size distributions can be combined into one compact, stack mountable instrument using a continuous microwave plasma torch operating in undiluted stack exhaust or air. First we briefly review the hardware details and the past field results for monitoring Cr, Be, and Pb total metals concentrations in an EPA test incinerator stack. Next, recent laboratory results are described for Cd, and Hg monitoring showing how low detection limits in air plasmas can be obtained. Finally, the potential for real-time particulate size distribution measurements is pointed out in the earlier field data and in the more recent laboratory signals taken with rapid time resolution.

1.3 Hardware

The major hardware elements of the microwave plasma continuous emissions monitor (CEM) for metals are shown in Figure 1-1. This system has been described in detail previously[1,2] and just a brief review is given here. The heart of the system is a microwave generated plasma sustained by a 1.5 kW, 2.45 GHz magnetron source with circulator and three stub impedance tuner from ASTex, Inc. The plasma in sustained inside a 25 or 28 mm internal diameter quartz or boron nitride tube which penetrates a shorted WR-284 (72 x 34 mm) waveguide through the center of its wide walls approximately one quarter wavelength (53 mm) back from the short. A narrowed waveguide (72 x 17 mm) has also been used to allow easier start up and stable operation at lower power (< 900 W) in air. Unlike all previously described analytical microwave induced plasmas (MIPs)[10,11] there is no resonance cavity. The microwave power is beamed directly into the plasma flame without obstruction making for very efficient microwave to plasma coupling at high power. Without adjustment of the three stub tuner coupling efficiencies are > 90% and approach 100% with adjustments. The plasma flame tends to fill the quartz or boron nitride tube and extend both upstream and downstream from the waveguide for total axial lengths in the 100 to 200 mm range, depending on the gas flow settings.

The sample gas to be monitored is introduced into the plasma by a 6.3 mm internal diameter quartz tube about 10 cm upstream of the waveguide. At the point that this tube enters the larger diameter plasma chamber, small tangential gas jets along the inside wall introduce a swirl gas flow which keeps the plasma flame off the wall. The plasma can be sustained over a wide range of sample gas flow of 0 – 30 liters per minute (lpm) corresponding to sample line gas velocities of 0 - 16 m/s (0 – 52 ft/s). Nominal sample gas flow used for most metals monitoring was approximately 14 lpm (24 ft/s) with a swirl gas flow somewhat less at about 10 lpm. A suction pump on the plasma exhaust establishes an isokinetic draw of the sample gas when this system is mounted on a stack. Both, a mechanical pump with heat exchanger[1] and a Penberthy jet pump[3] without moving parts have been used for this application. The exhaust is returned to the stack downstream of the sample collection line. For most laboratory measurements the sample and swirl gases come from pressurized sources and the suction pump is not used.

A unique feature of the microwave plasma CEM is a branch in the sample line with an attached span calibration system. An aerosol containing a known trace of metals can be momentarily turned on to flow into the sample line whenever needed to check monitor response. A Meinhard pneumatic nebulizer connected to a spray chamber, which filters out the large droplets, generates the aerosol. The nebulizer is operated with a controlled 1 lpm nitrogen gas flow which causes an uptake of approximately 1 milliliter per minute of standard solution containing the metals for which the CEM is to be calibrated. The metals transport efficiency from the standard solution to the sample line is calibrated off line by collecting filter samples and generally falls in the 0.3 – 0.9% range for this type nebulizer.

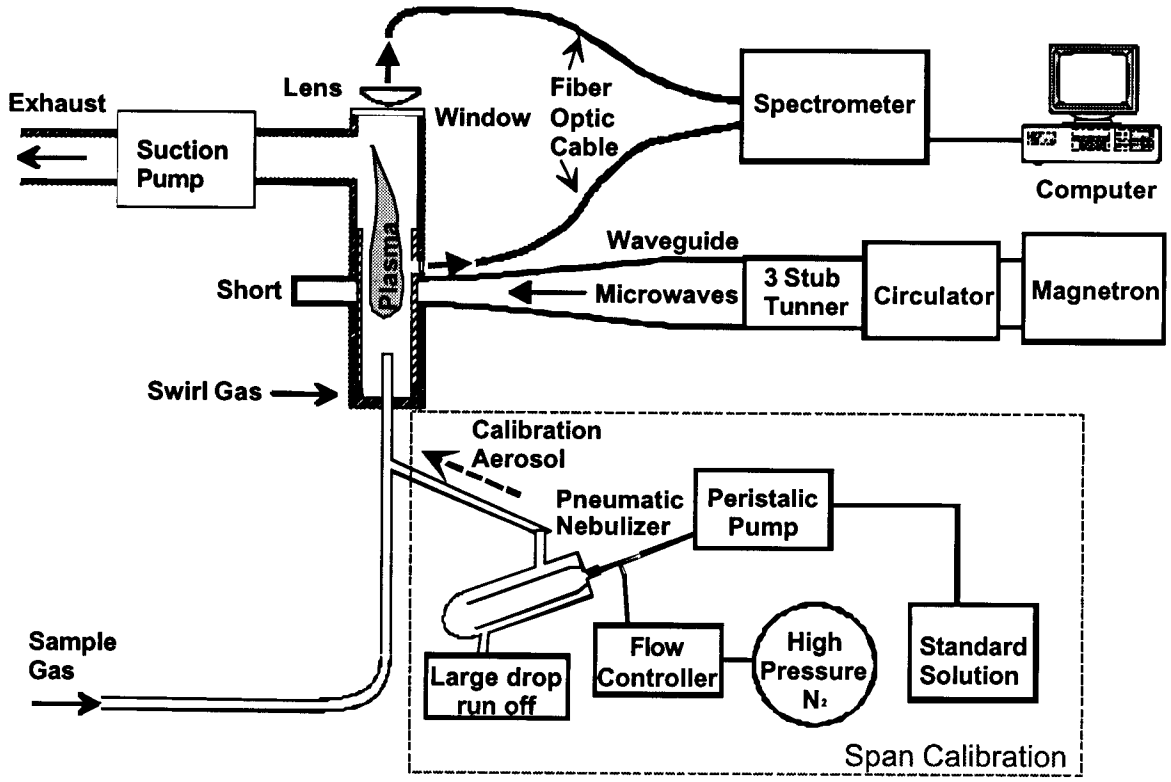

Figure 1-1. Block diagram of main components of the real-time calibrated microwave plasma CEM for metals.

The plasma emission light is viewed either axially from the entire plasma column or radially just upstream of the waveguide through fused quartz windows and lenses. Large core (0.8 – 1.0 mm), UV grade fiber optic cables of 1 to 3 meter lengths transport the light to spectrometers for analysis of the metals concentrations. A number of different commercial and custom fabricated grating spectrometers have been used to simultaneously monitor different metals[1, 2, 12]. In most cases, linear ccd and silicon diode detector arrays are used to monitor the strong metal emission transitions along with the plasma background spectrum around these transitions. Spectral data is acquired rapidly, several times a second, and processed in real-time for background emission[2]. A computer is used to display and store the resulting metal concentrations.

1.4 Past Stack Results

In September 1997 the microwave plasma CEM was implemented on a stack at the rotary kiln incinerator simulator facility at the EPA National Risk Management Laboratory in Research Triangle Park for a two-week testing period. These results have been described previously[1, 2, 13] and are briefly reviewed here to demonstrate the stack mounted capability for sensitive and accurate metal concentration measurements. The results also demonstrate the unique capability of this CEM for **true continuous** (100% on line duty factor) rapid sub-second data acquisition. In addition, the robustness of the microwave plasma flame was show by operating reliably with good metals sensitivity on an undiluted slipstream that was 6% water vapor.

At the time of the stack implementation the microwave plasma CEM was ready only to monitor three of the fourteen TRI metals. These were beryllium, chromium, and lead. A total of twenty stack exhaust tests were carried out with fly ash and aerosolized solution containing the test metals introduced into the exhaust. Ten tests were at high concentration of 40-60 $\mu g/m^3$ (actual) and ten tests were at low concentration of 10-15 $\mu g/m^3$ (actual). Two Method-29 (collection of stack samples in filters followed by laboratory analysis) reference measurements located on the stack upstream from the microwave plasma CEM were made for each test and averaged for relative accuracy calculations.

The microwave plasma light emission was monitored axially for all the tests. The lead emissions data for the third low concentration test is shown in Figure 1-2. It is typical of the data for the other metals and tests. The lower plot shows the raw data as it was acquired at 5 times per second. At this time resolution the low background lead concentration due to the stack injection of the aerosol solution can not be resolved because of the statistical signal fluctuations. The prominent features are the discrete fly ash transients due to lead containing particles as they pass through the system and the span calibration bumps, at a concentration of 92 $\mu g/m^3$, which where intentionally turned on at the two times indicated. This plot has a much higher y-axis concentration scale than the other two plots.

The middle plot of Figure 1-2 shows the same data after it has been smoothed to a 6-second time resolution. The steady background lead concentration at 11.5 $\mu g/m^3$ is now evident as well as the times when the aerosol metals stack spiking was interrupted and turned off. The fly ash spiking was not turned off between tests. At this time resolution the fly ash transients are mostly averaged out and do not contribute significantly to the total lead emission. Further smoothing of the data to one minute time resolution is shown in the top plot. The detection limit, defined as three times the standard deviation of the statistical signal fluctuations, improves inversely as the square root of time resolution from approximately 50 $\mu g/m^3$ in the lower plot to about 3 $\mu g/m^3$ in the upper plot. It is possible to continue smoothing the data to longer time resolutions to obtain even lower detection limits, but at some point 1/F noise will bound the ultimate achievable detection limit. This boundary has not been determined for the present system, though going out to two minutes smoothing to reduce the detection limit another factor of $\sqrt{2}$ is possible.

The top plot of Figure 2 also shows the accuracy relative to Method-29. The reference methods produced only one point over the time period of each test, which is plotted as a dashed horizontal line superimposed on the microwave plasma data. In this particular test there was exact agreement between the microwave plasma CEM and the reference methods. Not all the tests were as in good agreement, but quite a few were. A relative accuracy (RA) evaluation of all the tests resulted with RA values of about 20% for lead and beryllium and about 40% for chromium[1, 2]. The error was systematic to lower values for the microwave plasma CEM and could be an artifact of a cold finger in the stack between the microwave plasma and the upstream location of the reference methods[2].

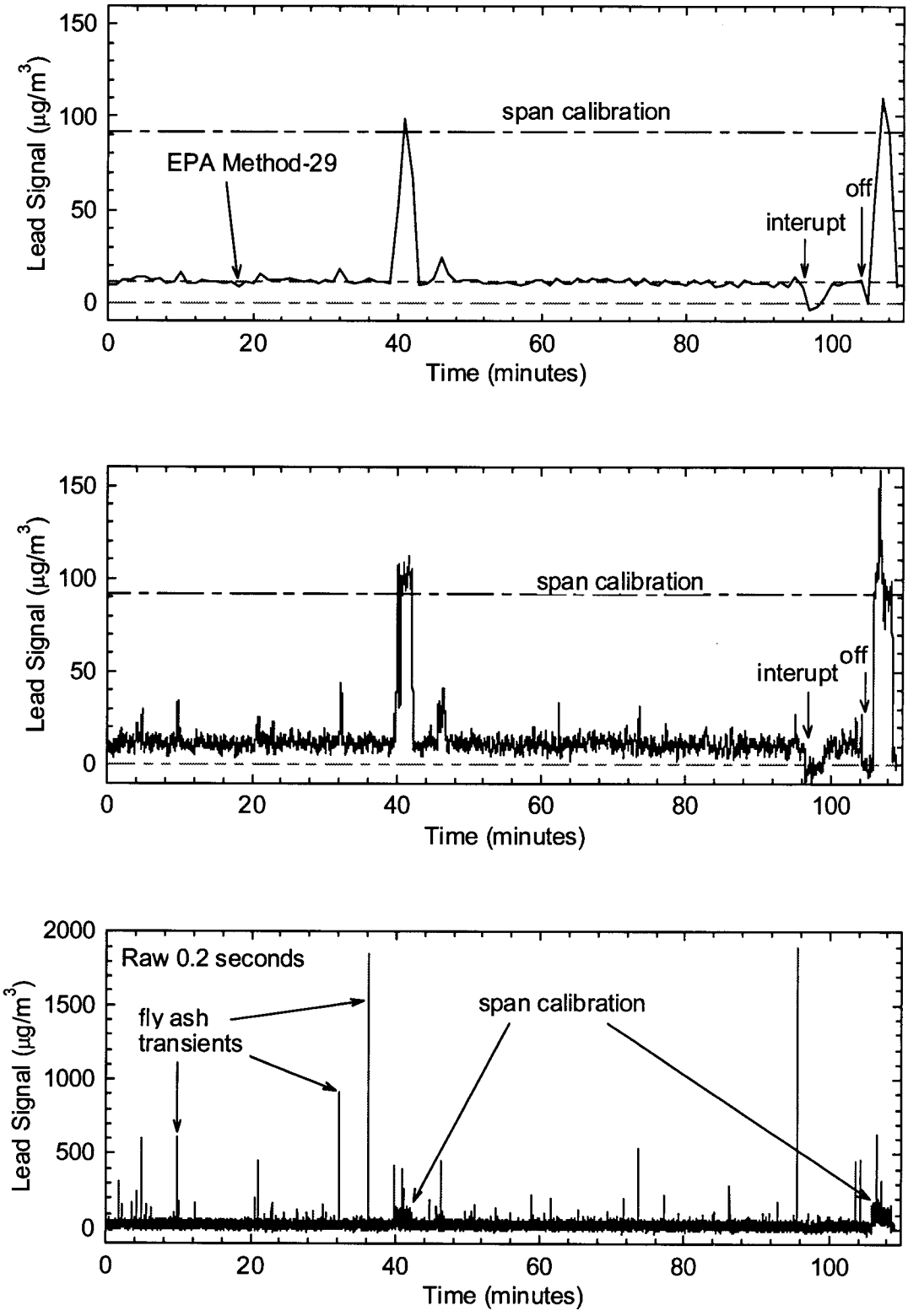

Figure 1-2. Stack test result for lead for the third low concentration run.

1.5 Recent Laboratory Results

Continued laboratory development of the microwave plasma CEM has focused on lowering the detection limits for cadmium and mercury. Plasma operation in a gas matrix of air or undiluted stack exhaust is not an optimum one for the detection of some metal atomic emission transitions. This is particularly true for atomic transitions that have a high excitation energy and those that terminate on the ground state. The electronic excitation temperature tends to be lower in molecular gas plasma, especially if oxygen is present. Studies of the microwave plasma have shown a dramatic increase in the detection limit of mercury on its usually strong 253.65 nm (excitation energy 4.89 eV) transition with just a small addition of oxygen (< 0.1%) to a nitrogen plasma[4]. The same is true for the usually strong 228.80 nm (excitation energy 5.42 eV) transition of cadmium. The observed reduction in emission for mercury was not due to the creation of a new UV absorption species in the plasma such as ozone [4].

The likely effect of adding a molecular species such as oxygen to the plasma is to reduce the population of energetic electrons that excite the high energy levels. Reduced excitation not only reduces the number of emitting atoms but also increases the number of unexcited atoms that can reabsorb the emission. Therefore, a slight decrease in excitation of an allowed atomic transition that terminates on its ground state causes a much greater decrease in its emission due to the concurrent effect of self-absorption. Self-absorption was observed in an air microwave plasma and is shown in Figure 1-3 for the 228.80 nm cadmium emission. The lower plot in Figure 1-3 is for an axial view that is 10 cm longer than for the upper plot. With the longer light propagation path length through the plasma flame self-absorption becomes so strong that the 228.80 nm emission becomes an absorption feature. The adjacent 226.50 nm transition remains an emission feature because it is due to an ionized state and therefore is not absorbed by unexcited cadmium.

The strategies for improving the detection limit of metals that are adversely effected by a molecular species in the plasma are: 1) use an atomic emission transition that is not a strong absorber in its ground state or, 2) make the light propagation path as short as possible through unexcited regions of the plasma. The first strategy was effectively used for cadmium because cadmium has a number other prominent transitions that can be used for detection. Though the 226.50 nm transition shown in Figure 3 was a candidate, a better one in the present microwave plasma proved to be the 326.1 nm (excitation energy 3.80 eV) transition. A detection limit of 8 $\mu g/m^3$ was achieved for one-minute time resolution in air at 14 lpm sample flow with an unoptimized spectrometer[5].

In the case of mercury the second strategy had to be used because there were no alternatives to the 253.65 nm transition in the present microwave plasma. The light propagation path length was made shorter by more than a factor of ten by viewing the emission from the side as shown by the side fiber optic in Figure 1. The view was put as close as possible to the microwave waveguide driven region of the plasma where the electron energies would be expected to be highest. Furthermore, the swirl gas was

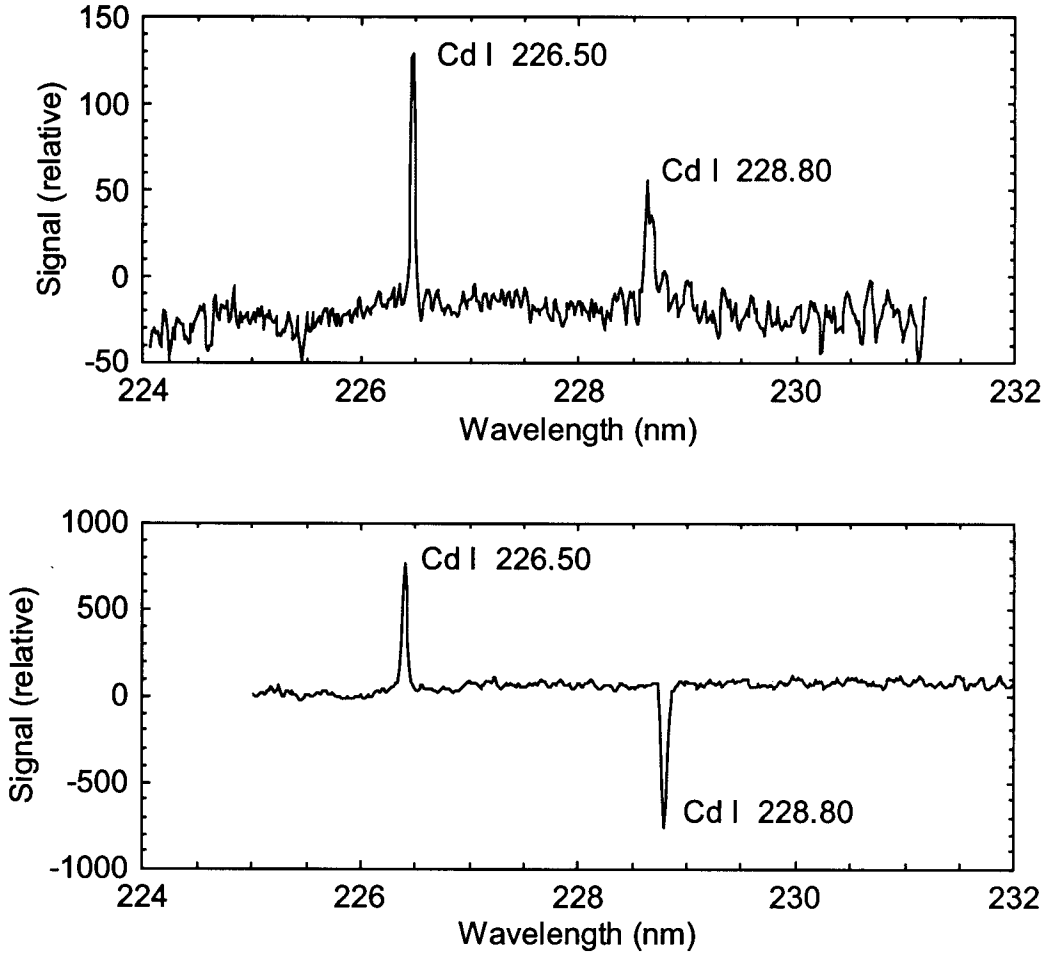

Figure 1-3. Cadmium spectra showing emission and self-absorption. Bottom spectrum is for a longer light propagation path length through the plasma.

changed to nitrogen rather than air which increased the mercury signals by removing the effects of oxygen in the plasma edges through which the light emission was viewed.

With the optimized side viewing geometry and an optimized spectrometer a study of the mercury detection limits versus gas flow was carried out at a microwave power of 1.5 kW. The results are shown in Figure 1-4. Mercury detection limits for one-minute time resolution are shown versus the sum of the sample and swirl gas flows. The sample flow volume varied from a minimum of 5 lpm to a maximum of 14 lpm in this data set with the swirl volume less than or about equal to the sample flow. The lower trace is for an aerosolized mercury salt from a weak HNO_3 acid solution injected into a nitrogen sample gas flow. The upper plot is for the same salt in an air sample gas. The swirl gas in both cases is nitrogen. At the lower sample flow the detection limits are about 0.2 and 1.0 $\mu g/m^3$ for the nitrogen and air plasmas, respectively, and increase to about 0.5 and 1.7 $\mu g/m^3$ at 14 lpm and low swirl flow. This is better sensitivity than current commercially available mercury CEMs that can only detect mercury[13].

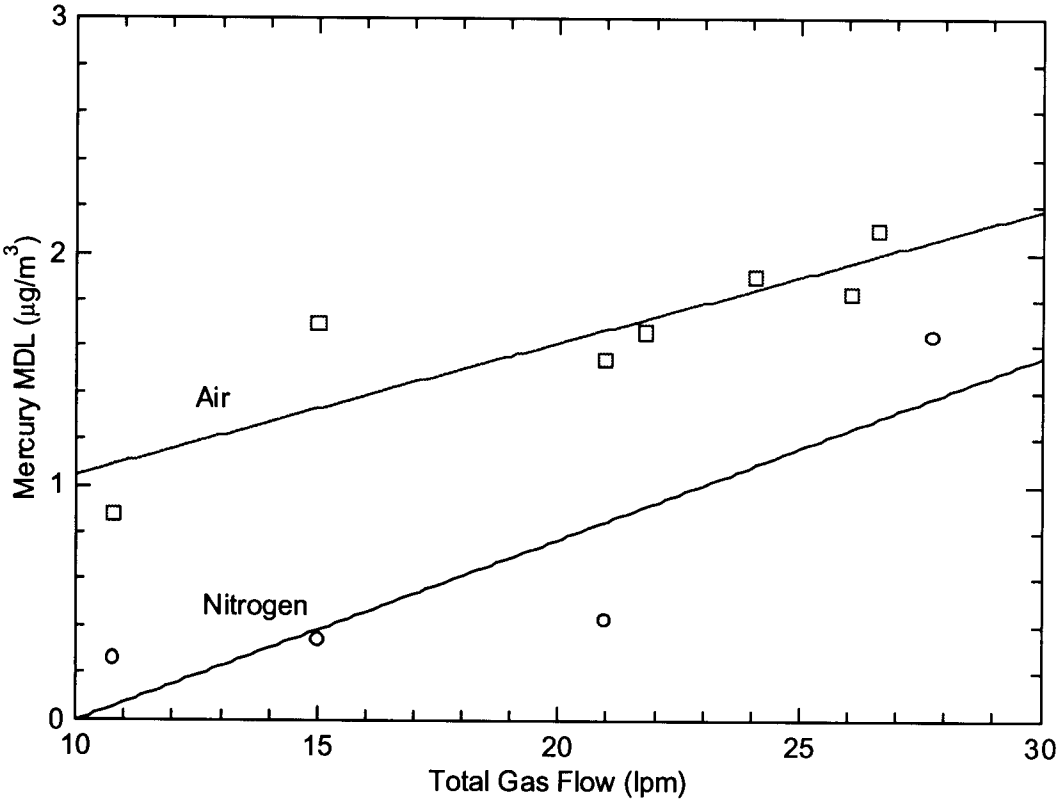

Figure 1-4. Mercury detection limits in air and nitrogen plasmas as a function of the sum of sample and swirl gas flow.

1.6 Potential for Particulate Measurements

The mode of operation of the stack mounted microwave plasma described here provides the capability to monitor particle numbers and size distributions. As shown in the discussion of past stack results the microwave plasma operates in true continuous mode (100% duty factor) with rapid sub-second signal acquisition. Consequently it resolves and detects every particle entrained in the gas flow passing through the plasma.

The prominent lead containing particles are evident in the bottom graph of Figure 1-2. In Figure 1-5 the iron signal at 360.88 nm recorded at the same time is shown. The amount of iron present in the fly ash of this stack test was many thousands of times larger than the hazardous metals. If the lower trace in Figure 1-2 is plotted on the same light emission scale in Figure 1-5, the highest lead transients would be lost within the first two tick marks of the iron graph. As expected there are many more, and larger, iron particles than those with lead. The mean size of the fly ash particles was 6 µm. This data demonstrates that, with some additional work, the stack mounted microwave plasma can be adapted to monitor and characterize particle distributions.

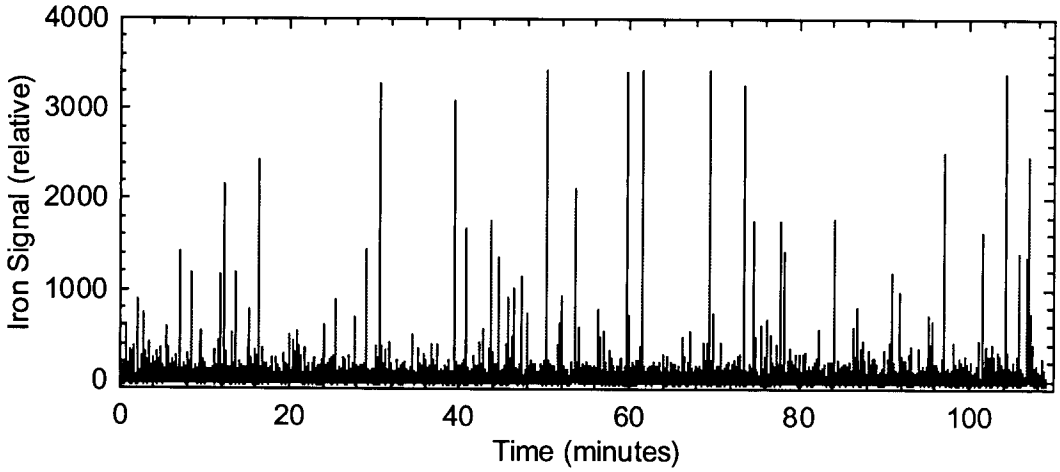

Figure 1-5. Iron emission data taken at the same time as the lead data in Figure 2.

However, there is a unique feature to this capability. The individual particles become visible by a mechanism that is significantly different from conventional particle monitors. There is no external light source. The particles are induced by the plasma to emit light. Consequently the discrete particle size that can be observed is not constrained by Mie or Raleigh scattering theory. Much smaller particle sizes can be monitored along with the larger ones. It should be possible to discretely monitor all particle sizes down to fine (< 2.5 μm) and ultrafine (< 0.1 μm) sizes for which commercially available monitors are not currently available.

Evidence for observing sub-micron particles is given in Figure 1-6. Axially viewed Microwave plasma emission light is shown at a wavelength of 326.106 nm corresponding to the wavelength of the strong cadmium transition. The span nebulizer was used to introduce an aerosol into the plasma and the signal was acquired at approximately 7 times a second. A heater tape around the sample line raised the temperature above 100 °C to prevent liquid droplets from entering the plasma. It has been shown that the particle salts generated by a nebulizer in this way are much smaller than 1 μm^8. In the first half of the trace in Figure 6 a blank solution is used and then, where indicated by the arrow, replaced by a solution containing a weak HNO_3 acid solution with cadmium. The inherent fine to ultrafine particulate nature of the cadmium introduced into the plasma is evident by the significant increase in the signal fluctuations when the metal salt is present. This behavior is typical for other metal aerosols too.

The axial optics for the data in Figure 1-6, and also for the data in Figures 1-2 and 1-5, viewed most of the plasma volume (~50 cm^3) and therefore particle overlap is significant. A different viewing optics arrangement to view a much smaller volume would be able to observe discrete fine and ultrafine particles. Diffraction limited viewed volumes factions of a cubic millimeter are possible. With optimized viewing geometries the microwave plasma would make possible monitoring discrete particles over a dynamic range of sizes much greater than currently possible.

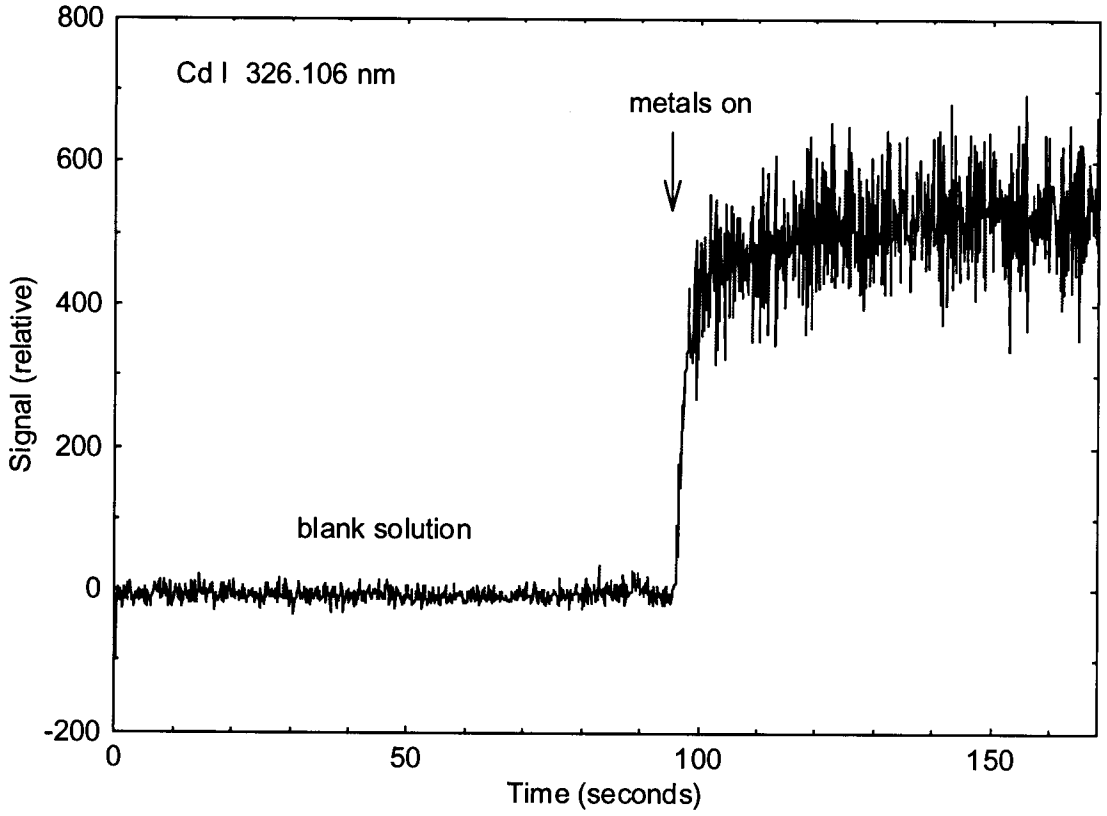

Figure 1-6. Evidence of sub-micron particle resolution when aerosolized metal salts are present in the plasma.

1.7 Conclusions

The compact, stack mountable microwave instrumentation described here with its attached span calibration system and fast signal acquisition represents a significant advance in stack emissions monitoring capability. The results to date show that 2.45 GHz microwave power (≤ 1.5 kW) in a simple shorted waveguide can sustain a reliable, continuous (100% on line duty factor), large volume (~50 cm^3) plasma in a stack slipstream (or inside the stack[3]) for atomic emission spectroscopy of stack emissions. Good measurement accuracy (RA ≤ 20%) for metals concentration is readily achieved with the attached span calibration injector. By this method measurement accuracy can be maintained over variable exhaust gas-matrix conditions and other field variables such as optics cleanliness and electronic drifts. Tests at an EPA research incinerator with reference Method-29 have confirmed the capability for accurate measurements. In addition these test have shown low detection limits < 3 $\mu g/m^3$ for Be, Cr, and Pb for one-minute time resolution in undiluted stack exhaust plasmas having a 6% content of water.

Recent laboratory development has overcome the difficulties with monitoring mercury in an *in situ* or near *in situ* plasma gas matrix by determining the plasma mechanisms that limit Hg 253.65 nm emission. These mechanisms were identified as reduced electronic excitation and self-absorption. As a result of this knowledge the collection optic views and spectrometer configuration have been reengineered to improve performance. A one-minute mercury detection limit in an air plasma of $\leq 1\ \mu g/m^3$ has been achieved in the laboratory. Though a stack test will be needed to confirm this performance in the field, even with some degradation this level of performance rivals the best capability of currently available commercial technologies than can detect only mercury in more complex instrumentation packages.

The microwave plasma monitoring capabilities described here go beyond metals concentration measurements. Because of the fast signal acquisition, particle size distributions and discrete particle elemental compositions can be observed. Much smaller particle sizes can be observed than has been previously possible because of the fundamentally different nature by which the particles are made visible. They are induced by the plasma to be sources of light rather than passively scattering, shadowing, or diffracting light from an external source. The usual limits on particle size resolution are thus avoided. For the first time a potential continuous capability to monitor fine and ultrafine particulate matter has been demonstrated without compromising the ability to observe larger particles. Human respiratory deposition/dose of hazardous chemicals depends in part on the particulate size distributions so such measurements are important to assess the full impact of emissions on human welfare.

As public concern and government regulations increase to control and monitor stack emissions of potentially polluting processes, there will be a growing need for real-time emissions monitoring technologies for numerous emissions parameters and chemicals. Monitoring technologies that can provide measurements of multiple parameters and chemicals would represent a significant cost savings and reduction in complexity of stack implementation. Such technologies would also be of value in researching sources of emissions to provide an understanding for improving processes for reducing emissions. The microwave-plasma monitoring technology described here, when fully developed, could make a significant contribution in that direction.

1.8 References

1. P. P. Woskov, K. Hadidi, P. Thomas, K. Green, and G. J. Flores, "Accurate and sensitive metals emissions monitoring with an atmospheric microwave-plasma having a real-time span calibration", J. Waste Management, to be published, May 2000. www.psfc.mit.edu/library/99ja/99ja011/99ja011_abs.html

2. P. P. Woskov, K. Hadidi, P. Thomas, K. Green, G. J. Flores, and D. A. Lamar, Field "Test of a Real-Time Calibrated Microwave Plasma Continuous Emissions Monitor for Stack Exhaust Metals", MIT Plasma Science and Fusion Center Report PSFC/RR-98-1, February 1998. www.psfc.mit.edu/library/98rr/98rr001_abs.html

3. P. P. Woskov, D. Y. Rhee, P. Thomas, D. R. Cohn, J. E. Surma, and C. H. Titus, "Microwave plasma continuous emissions monitor for trace metals in furnace exhaust", Rev. Sci. Instrum., vol. 67, 3700-3707, 1996.

4. K. Hadidi, P. P. Woskov, G. J. Flores, K. Green, and P. Thomas, "Effect of oxygen concentration on the detection of mercury in an atmospheric microwave plasma", Japanese J. of Applied Physics, vol. 38, 4595-4600, 1999.

5. K. Hadidi, P. P. Woskov, K. Green, and P. Thomas, "Observation of Self Absorption of Hg I and Cd I Emission in an Atmospheric Microwave Sustained Plasma", MIT Plasma Science and Fusion Center Report PSFC/JA-99-98, 1999. www2.psfc.mit.edu./library/99ja/99ja028/99ja028_abs.html

6. D.K. Ottesen, J.C.F. Wang, and L.J. Radziemski, "Real-Time Laser Spark Spectroscopy of Particles in Combustion Environments", Applied Spectroscopy, vol. 43, 967, 1989

7. C.A. Noble and K.A. Prather, "Real-Time Measurement of Correlated Size and Composition Profiles of Individuals Atmospheric Aerosol Particles", Environmental Science Technology, Vol. 30, p. 2668, 1996.

8. D.W. Hahn, "Laser-induced breakdown spectroscopy for sizing and elemental analysis of discrete aerosol particles", Appl. Phys. Lett., vol.72, pp.2960-2962, 1998.

9. H. Takahara, M. Iwasaki, and Y. Tanibata, "Particle analyzer system based on microwave-induced plasma technology", IEEE Trans. Instrum. and Meas., vol.44, pp.819-823, 1995.

10. M. W. Blades, P. Blanks, C. Gill, D. Huang, C. Le Blanc, and D. Liang, "Application of weakly ionized plasmas for materials sampling and analysis", *IEEE Trans. on Plasma Sci.* **19**, pp.1090-1113, 1991.

11. J. P. Matousek, B. J. Orr, and M. Selby, "Microwave-Induced Plasmas: Implementation and Application", Prog. Analyt. Atom. Spectrosc., vol. 7, 275-314, 1984.

12. 1997 Performance Testing of Multi-Metals Continuous Emissions Monitors, DOE/ID-10665, Idaho National Engineering & Environmental Laboratory, September 1998.

13. N. B. French, S. J. Priebe, and W. J. Haas, Jr., "State of the Art Mercury CEMs", Analytical Chemistry News & Features, 470A –475A, July 1, 1999.

2. Effect of Oxygen Concentration on the Detection of Mercury in an Atmospheric Microwave Discharge

K. Hadidi, P.P. Woskov, G.J. Flores, K. Green, P. Thomas

Plasma Science and Fusion Center, Massachusetts Institute of Technology
Cambridge, MA 02139, USA

2.1 Abstract

A microwave plasma combined with atomic emission spectroscopy is being developed for real time emission monitoring of metals in smokestacks. The plasma is sustained by 1.5 kW, 2.45 GHz microwave radiation in a gas flow at atmospheric pressure. The addition of oxygen to a nitrogen gas stream reduces dramatically the emission intensity of the 253.65 nm mercury transition, while at the same time it increases the emission intensity of the 405.78 lead line and other metal transitions. Measurements as a function of oxygen concentration in the plasma gas stream on the intensity of the 253.65 nm mercury line and on the excitation temperature, T_{exc}, are presented. Possible mechanisms in the plasma that can effect the emission strength of the Hg atom are explored. Plasma absorption at 253.65 nm by ozone is ruled out by UV transmission measurements. The measurements suggest that a slight cooling of T_{exc} with the addition of oxygen, combined with the sharp electron impact excitation cross section can explain the observed behavior.

KEYWORDS: Emission monitoring of metals, mercury detection, smoke stacks, atmospheric microwave discharge, excitation temperature

2.2 Introduction

Throughout the world, legislation is being tightened to reduce the emission of hazardous metals such as mercury and arsenic from power plants, thermal processing plants, and other industrial sources. In the USA, the Environmental Protection Agency (EPA) is planning to tighten emission regulations of at least 7 of the most hazardous metals (Hg, As, Sb, Pb, Be, Cr, and Cd). However, to enforce the new proposed laws, measurement instrumentation must be made available to these industries to insure compliance with the new emission limits. At the present time, there is only one commercial real time metals monitoring system available on the market[1]. Improvements are still needed in measurement accuracy, sensitivity, and affordability. Several methods that make use of plasmas for atomic emission spectroscopy (AES) of trace metals are being developed to address this need for real time monitoring of heavy metals in smoke stacks. Some of these methods such as inductively coupled plasma (ICP)[2,3] and laser induced breakdown spark (LIBS) systems[4,5] have some limitations. In the case of ICPs they either require high power (more than 2 kW) and/or special gases such as argon or helium. In the case of LIBS they analyze a very small volume of the stack gas (few cubic micrometers) in situ for very short time pulses (a few microseconds) which limits sensitivity and may not be representative of the bulk gas. These methods have also not been able to consistently achieve EPA's goal of 20% relative accuracy to EPA's current reference method using collected stack samples of metals content.

At the Plasma Science and Fusion Center at MIT, a microwave sustained plasma is being developed for real time atomic emission spectroscopy of trace metals in stack exhaust[6]. Unlike other microwave plasma element analysis systems that make use of a surfatron[7], a resonant cavity[8] or an Okamoto cavity[9] to sustain a plasma, the MIT system uses a non-resonant shorted waveguide. This allows operation of a very stable and efficient plasma in air and undiluted stack exhaust at moderate powerlevels (0.5-1.5 kW) and at high flow rates (>12 l/min). Excellent minimum detection limits have been achieved in air and undiluted stack exhaust plasmas for Pb, Be, and Cr[10]. Good detection limits have also been achieved for Cd, Hg, and As in pure nitrogen and noble gas plasmas. However, the detection limit for Hg and As has been found to degrade significantly in an air plasma.

The purpose of the present study is to attempt an understanding of why the mercury emission light at 253.65 nm is significantly decreased in a microwave sustained air plasma at atmospheric pressure. The present study has focused on the role of oxygen in the plasma. In the case of arsenic detection at UV wavelengths < 200 nm, oxygen absorption of the UV light can explain the reduced light emission. However, plasma absorption at 253.65 nm has been ruled out for the case of mercury by the measurements presented here. Other researchers have also found that the addition of some compounds containing oxygen such as carbon dioxide and water vapor to an argon-nitrogen plasma decreases the mercury light intensity to a considerable extent[11]. Also, J.F. Camuna-Aguilar et al.[12] describe the effect of water on the mercury signal in an argon and helium microwave induced plasma.

2.3. Instrumentation

A schematic diagram of the equipment used in this experiment is given by Figure 1-1.

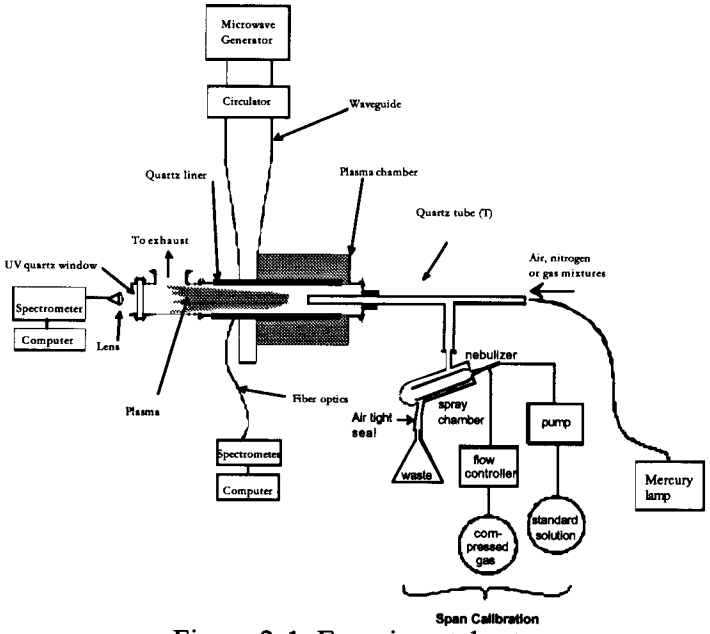

Figure 2-1. Experimental setup

The microwave source is a 2.45 GHz magnetron from Astex Inc., with a maximum power of 2.5 kW. The microwave radiation travels inside a standard WR-284 brass waveguide which is tapered to inside dimensions of 19.1 x 76.2 mm with a short at the tapered end. A 31.8 mm hole traverses the wide waveguide walls a quarter wavelength back from the short. The plasma discharge is started by a 15 kV electric spark between two tungsten electrodes located just up stream of the waveguide inside the plasma chamber and connected to a high voltage transformer. The plasma is then sustained by the microwave radiation and maintained inside a 25.4 mm id boron nitride tube in the chamber. It is kept from the walls by a swirl jet of air or nitrogen.

A suction pump draws a gas sample through a 6 mm id quartz Tee which is inserted into the plasma chamber. After passing through the plasma, the gas is cooled down in a heat exchanger before it goes into the suction pump, then out to the exhaust hood. Metallic aerosols such as mercury are injected into the plasma chamber through the quartz Tee by a Meinhart pneumatic nebulizer with an injection rate of 1 ml/min and an efficiency of ~0.9%. A 10,000 μg/ml ICP standard Hg solution in 5% HNO_3 is used as the source of mercury. For iron and lead, a 1000 μg/ml solution is used. The nebulizer is calibrated against a "rod-insertion calibration method" developed in the laboratory[13]. On the plasma axis and at a distance of 25 cm from the waveguide, there is a quartz window and a lens that takes the light from the plasma and concentrates it outside at the lens focal length (75 mm). A one or two meter long UV fiber optic is mounted at the focal point and is connected to an Instruments S.A. Model THR-640 spectrometer. This instrument has a 2400 groove/mm grating, adjustable slit, and a Princeton Instruments Model IRY-512W

intensified 512-element detector array. The spectral resolution is about 0.05 nm with an instantaneous spectral range of about 6.5 nm that can be tuned from 180 to 600 nm. When nitrogen spectrum is studied, a custom spectrometer with higher resolution is used to distinguish between the P and R branch lines. This instrument has a 3600 groove/mm grating, 0.84 m focal length, and a 2,048 element StellarNet CCD detector array. It is capable of a maximum spectral resolution of about 0.012 nm centered at 386 nm in one of its four instantaneous bands used for the present measurements[14].

Possible ultraviolet light absorption in the plasma at 253.65 nm was checked by transmitting light from a low-pressure mercury lamp axially through the length of the plasma as shown in Figure 1. The mercury lamp was a Model 6035 from Oriel Corp. The light from this lamp was directed by a fused silica fiber to the axial input of the Tee. For the UV transmission measurements the span calibration system was removed to allow the introduction of the axial flow gas into the plasma through the side port of the Tee. The air, nitrogen, and oxygen gas flows were independently controlled by calibrated flow meters at the input.

2.4 Experiments and Results

For all experiments, an aerosol of clean deionized water vapor is first injected into the plasma trough the nebulizer to acquire a background spectrum. An aerosol of the solution containing mercury is then introduced into the plasma. The water spectrum is used to subtract the effect of moisture on the mercury spectrum. It is assumed that the water spectrum is representative of the diluted HNO_3 acid spectrum. The base plasma gas flows are 14 liter per minute axial and 9 l/min swirl with pure nitrogen in both flows. Oxygen is then added into the axial flow through a very sensitive Omega Model 234 flowmeter. The ISA spectrometer is used to sequentially take 400 instantaneous spectrums at 100 ms/spectrum at each oxygen concentration. The data analysis consists of averaging the 400 spectrums for the background and for the signal with mercury injected into the plasma, then subtracting the averaged background signal from the averaged mercury signal. The minimum detection limit (MDL) is calculated as 3 times the standard deviation of the noise of the resulting signal and is given by the following formula:

$$MDL = \varepsilon \frac{3\sigma XR}{SF} \qquad (2\text{-}1)$$

where ε is the nebulizer efficiency, σ is the standard deviation of the noise taken on a background detector pixel as close as possible to the spectral signal peak, X is the standard solution concentration in μg/ml, R is the rate of solution in ml/min pumped into the nebulizer, S is the signal intensity in counts, and F is the volume flow rate of gas in the sample line in m^3/min.

Figure 2-2 shows the effect of adding oxygen to the nitrogen axial flow on the 253.65 nm mercury line emission intensity and its minimum detection limit. Mercury signal decreases and the detection limit increases as the oxygen content is increased in the axial flow gas. This effect has not been observed with lead and iron. In fact, the signal of lead on the 405.78 nm line increases slightly Figure 2-2. Effect of O_2 on Hg 253.65 nm with oxygen in the axial flow and the detection limit decreases as shown in Figure 2-3.

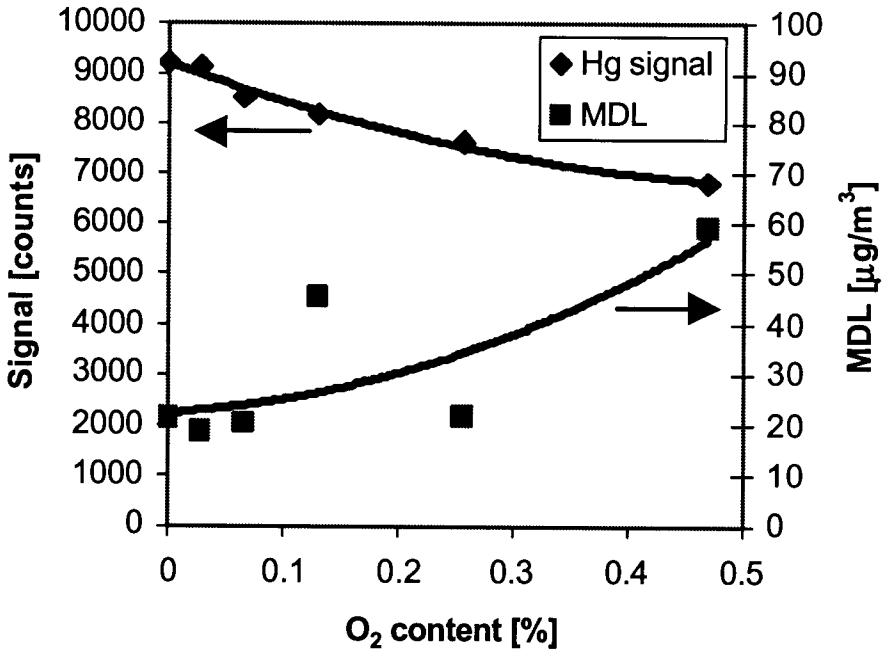

Figure 2-2. Effect of O_2 on Hg 253.65 nm signal and minimum detection limit.

From Figure 2-2, it appears that oxygen and/or an oxygen derived species such as ozone may be responsible for the decrease of Hg light emission in the nitrogen plasma. To understand this phenomena, we investigated the effect of oxygen on the rotational and the excitation temperatures. The excitation temperature is considered to be representative of the electron temperature.

2.4.1 Rotational Temperature Measurements

We measured the rotational temperature of the N_2^+ ion in the plasma by using the line pair intensity ratio method[15]. This method assumes a Maxwell-Boltzmann distribution of energy levels and takes the ratio of the light emission intensity between two spectral peaks to obtain a temperature. In our case one peak is taken from each of the R and P branches of the nitrogen ion molecule N_2^+. The line intensity for one peak is given by reference[16]:

$$I_{em} = \frac{C_{em}.n^4}{Qr}.(J'+J''+1)exp[-B'J'(J'+1)hc/kT] \qquad (2\text{-}2)$$

where I_{em} is the emission intensity of a given line, C_{em} is a constant depending on the change of dipole moment and the total number of molecules in the initial vibrational level, n is the wavelength, J' the upper level, J" the lower level, B' is the rotational

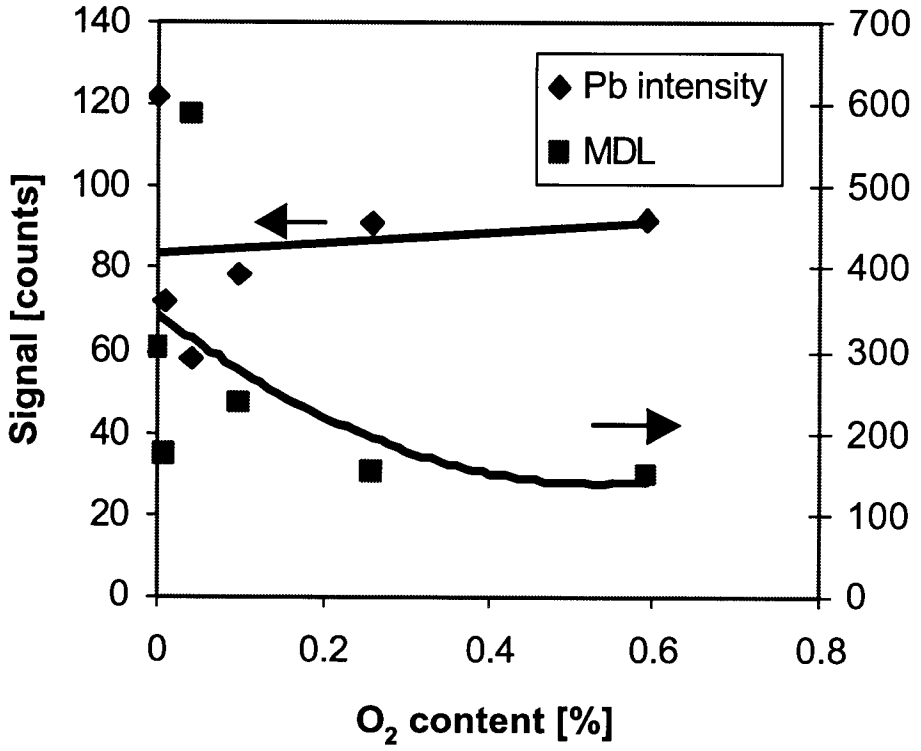

Figure 2-3. Effect of O_2 on Pb signal and minimum detection limit.

constant, and Q_r is the rotational partition function. By applying equation 2 to R29 and P56 peaks of the 0-0 band of the first negative system of N_2^+ and by taking the ratio of the two lines, we obtain the rotational temperature through the following equation

$$T_{rot}\,[K] = \frac{6421}{\ln\frac{I_{R29}}{I_{P56}} + 0.62415} \qquad (2\text{-}3)$$

These two lines were chosen because they almost overlap spectrally, but their energy levels are far apart. This minimizes the error in the temperature calculation due to spectral variation in the spectrometer response and due to experimental intensity measurement uncertainties.

For these rotational temperature measurements, we used the custom spectrometer described above. Figure 4 shows a partial spectrum of the N_2^+ first negative system 0-0 band and the two peaks, R29 and P56, used to calculate the rotational temperature. Equation 3 was applied to different spectra taken as a function of oxygen concentration in the plasma. The resulting rotational temperature is shown in Figure 2-5. A rotational temperature of 5000 K has been determined in an all nitrogen discharge, which is in agreement with the results of K. Ogura et al.[17] who measured the rotational temperature in a microwave-induced nitrogen plasma using an Okamoto cavity. From this figure, we can see that there is a slight drop in the rotational temperature when oxygen concentration increases in the plasma.

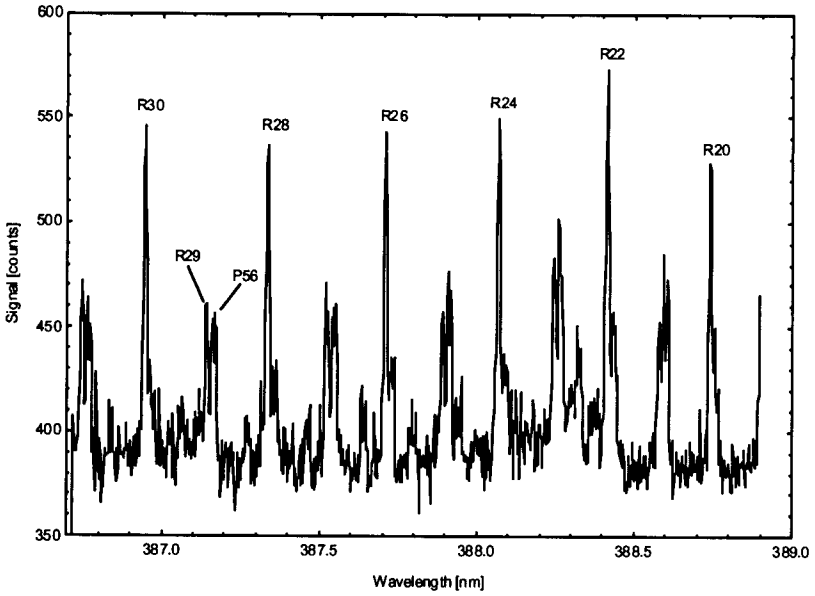

Figure 2-4. N_2^+ spectrum

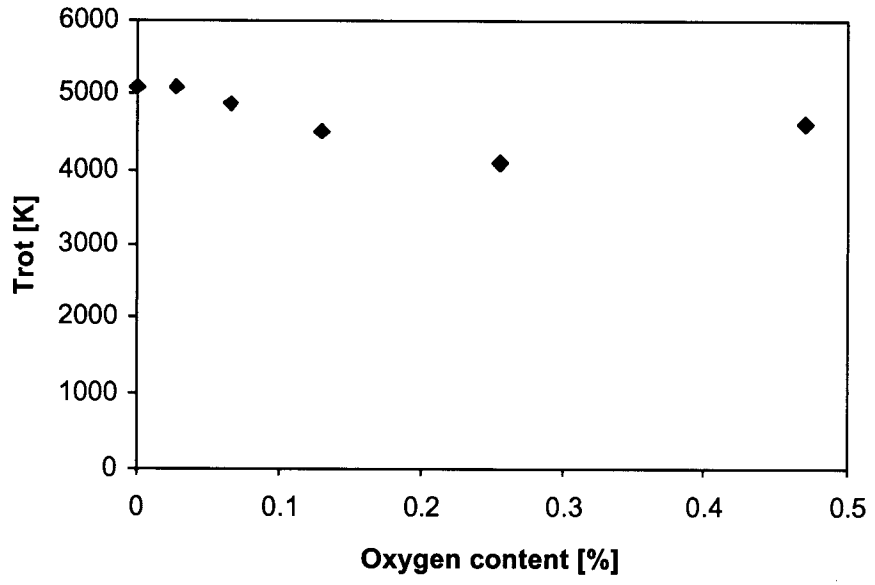

Figure 2-5. Rotational temperature

2.4.2 Excitation Temperature Measurements

The atomic excitation temperature has also been calculated assuming a Maxwell-Boltzmann distribution of the electronic energy levels. The slope of a log plot of emission intensity versus the energy of the excited level as related below gives the temperature[15].

$$\mathrm{Log}\left(\frac{I\lambda}{gf}\right) \alpha\, E_{exc} \qquad (2\text{-}4)$$

where I is the emission signal intensity, λ is the wavelength of the transition, g is the statistical weight, f the oscillator strength and E_{exc} is the excitation energy. The slope is related to theexcitation temperature by the following equation:

$$T_{exc} = \frac{-0.625}{\log\frac{I\lambda^3}{gf}} \bullet E_{exc} \qquad (2\text{-}5)$$

Because iron lines between 370 and 380 nm were too weak to use for temperature measurements in a pure nitrogen plasma, we used titanium lines covering an energy range from 30,837 to 43,781 cm^{-1} to measure the excitation temperature. The values of gf parameters are taken from Wiese and Furt[18]. Figure 2-6 shows the results as oxygen concentration is increased in a nitrogen plasma. The excitation temperature is within the limits of the results of K. Ogura et al.[17]. Even though the error margin is high, a slight decrease in the excitation temperature can be noticed on the curve.

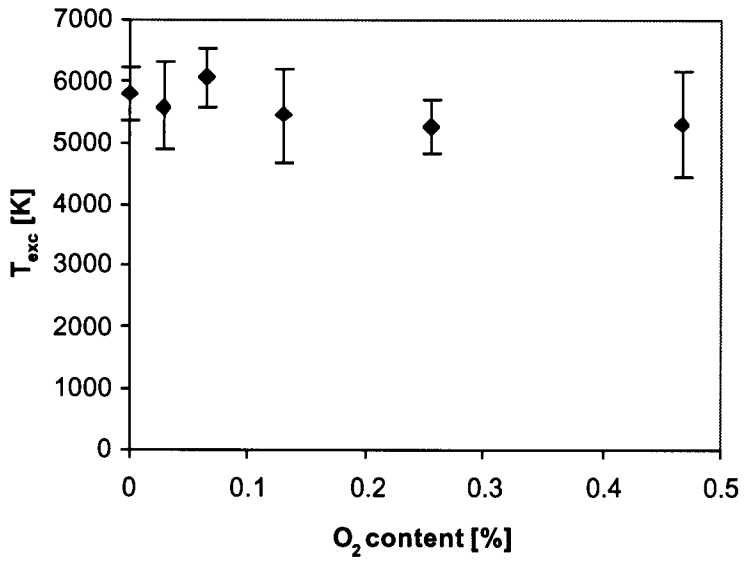

Figure 2-6. Excitation temperature

2.4.3 Absorption

Transmission measurements of 253.65 nm light from a low-pressure mercury lamp through the entire axial length of the plasma (~25 cm) as a function of oxygen concentration in nitrogen did not reveal any measurable increase in absorption at this wavelength. A slight increase in transmission was noted with a small addition (~ 2%) of oxygen, but at 20% concentration there was no difference, within experimental measurement error, in the UV transmission relative to a pure nitrogen plasma. The slight increase in transmission is probably due to a lensing effect along the plasma axis of propagation. This measurement shows absorption of the 253.65 nm mercury light by oxygen and/or oxygen derived compounds such as ozone is not the mechanism responsible for the decrease in mercury emission intensity when oxygen is added to the plasma.

2.5 Discusion

The results presented above clearly show that the addition of oxygen to a nitrogen plasma has an opposite effect on the light emission intensity of mercury at 253.65 nm and on lead at 405.78 nm as well as on other transitions of iron. Any explanation of the plasma mechanism that reduces the light emission of mercury by the addition of oxygen should not be in conflict with the fact that oxygen increases the light emission intensity of lead and iron transitions. The present experimental measurements restrict the possible explanations for the observed behavior of mercury emission in an atmospheric microwave plasma.

Selective absorption of the 253.65 nm mercury light by an oxygen species is ruled out by the UV transmission measurements. The fact that the measured rotational temperature, which is usually assumed to be the same as the gas temperature, is about 5000 K indicates that most of the oxygen molecules can be decomposed. This would allow the formation
of oxygen radicals, therefore producing ozone molecules in the after glow. It is well known that ozone strongly absorbs the 253.65 mercury line. However, the observed lack of absorption indicates that ozone is not present in the regions of the plasma and afterglow through which the spectrometer views emission. Since ozone decomposes at a temperature of 261.1 °C[19], this suggests that the plasma and adjacent regions being viewed are too hot for the formation of ozone.

Not tested by the present absorption measurement is the effect of trace mercury in the plasma. Absorption by unexcited mercury in the outer regions of the plasma chamber through which the plasma emission is viewed may be a factor in reducing observed mercury emission since the lower level of the 253.65 nm transition is the ground state. This by itself would not explain the observed change between a pure nitrogen and nitrogen with oxygen plasma having the same content of mercury. The explanation of the observed decrease in mercury emission with the addition of oxygen is most likely due to a reduction in the excitation of mercury when oxygen is present in the plasma.

Oxygen, having an affinity for electrons, may be expected to reduce the electron density in the plasma, therefore reducing the probability for a mercury atom to be excited by electron impact either directly or via a metastable state of another plasma species. This explanation is unlikely because electron impact, either directly or indirectly, is responsible for exciting all atomic species in the plasma. A reduction in electron density by itself would be expected to effect all atomic emission in the same way. This is not the case in the present observations. Lead and other metal emission line intensities increase opposite to the oxygen effect on mercury.

A change in the electron energy distribution or temperature with oxygen could account for the observed behavior of the metals emission. The electron impact cross-section for the excitation of the various mercury transitions as a function of electron energy is shown in Figure 2-7 [20]. The excitation curve for the strongest 253.65 nm transition is given along with the excitation curves for the 435.8, 407.8, 313.2, 313.2, 312.6, and 289.4 nm lines and their sum with the 265.4 nm line. The excitation cross-section for the 253.65 nm transition peaks at a very narrow electron energy bandwidth at 5.5 eV. This is much higher than the measured plasma excitation temperature of approximately 0.5 eV, which is considered an indicator of the mean electron energy. It is the energetic tail electrons of the electron energy distribution that excite mercury in this plasma. At the maximum cross section for the line at 253.65 nm, a decrease in the electron energy of 12.5% would cause a 50% decrease in the light intensity. Also, a slight decrease observed for the excitation temperature as shown in Figure 2-3 could indicate a larger reduction in energetic electrons. This may account for the observed decrease in signal intensity of the mercury line when oxygen is added to the nitrogen plasma. The other metals behave differently because their excitation cross-section may not be as peaked and shifted to lower energies.

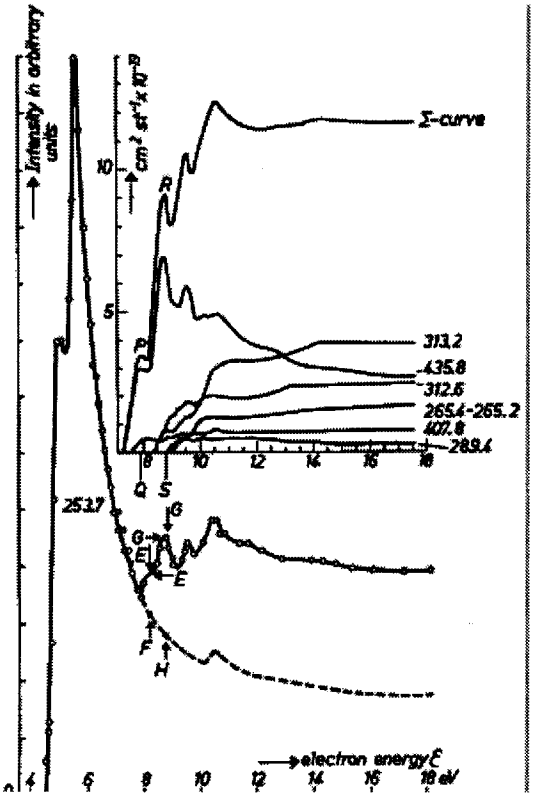

Figure 2-7. Electron impact cross-section for the excitation of the various mercury transitions as a function of electron energy (from ref. 20).

Another possible explanation for the observed behaviour of metals light emission is the selective quenching of excited mercury atoms by oxygen or oxygen derived species in the plasma. This possibility is a subject for future investigations.

2.6 Conclusion

This study has shown that oxygen addition to a nitrogen atmospheric plasma effects the light emission from mercury and lead in opposite ways. Mercury light emission of the 253.65 nm line is strongly reduced by the presence of oxygen in the plasma while the lead 405.78 nm line and some other metal lines are enhanced. Selective absorption of the mercury UV emission by oxygen or oxygen derived species in the plasma has been rule out by UV transmission measurements. It has been shown that oxygen slightly lowers the gas temperature and the excitation energy in the plasma. This effect in combination with the sharp excitation cross-section of mercury may account for the decrease in the light emission intensity of mercury with the addition of oxygen. An improved understanding of the plasma mechanisms that effect the emission intensity of mercury in

atmospheric plasmas is of va lue to the development of real time mercury trace metals pollution monitors.

2.7 References

1 G. A. Meyer, Proceedings of SPIE, Vol. 3534, Environmental Monitoring and Remediation Technologies, Boston, Nov. 1998.

2 C. Trassy, R. Diemiaszonek, P. Pasquini, and R. Meunier: Proc. Of Int. Sym. on Environmental Technologies, Plasma System and Applications, Atlanta, 1995, p. 401.

3 M. D. Seltzer and R. B. Green: Process Control and Quality. 6 (1994) No. 1, 37.

4 D. W. Hahn: Appl. Phys. Lett. 72 (1998), 2960.

5 J. P. Singh, Fang-Yu Yueh, Hansheng Zhang, R.L. Cook: Process Control and Quanlity 10 (1997), 247.

6 P.P. Woskov, D.Y. Rhee, P. Thomas, D.R. Cohn, J.E. Surma, and C. Titus: Rev. Sci. Instrum. 67 (1996), 3700.

7 M.H. Abdallah, S. Coulombe, and J.M. Mermet: Spectrochemica Acta 37B (1982), No. 7, 583.

8 K. Larjava, T. Laitinen, T. Vahlman, S. Artmann, V. Siemens, J.A.C. Broekaert, and D. Klockow: Intern. J. Environ. Anal. Chem. 49 (1992), 73.

9 Y. Okamoto: Anal. Sci. 7 (1991), 283.

10 P.P. Woskov, K. Hadidi, P. Thomas, K. Green, G. Flores, and D. Lamar: Massachusetts Institute of Technology, PSFC/RR-98-1, (1998).

11 V. Siemens, T. Harju, T. Laitinen, K. Larjava, and J.A.C. Broekaert: Fresenius J. Anal. Chem 351 (1995), 11.

12 J.F. Camuna-Aguilar, R. Pereiro-Garcia, J.E. Sanchez-Uria, and A. Sanz-Medel: Spectrochemica Acta 49B N0.5, (1994), 475.

13 G.J. Flores, K.M. Green, P.P. Woskov, K. Hadidi, and P. Thomas: 40th Annual Meeting of the Division of Plasma Physics of APS, Nov. 1998, New Orleans, LA.

14 P. P. Woskov, K. Hadidi, M. C. Borras, P. Thomas, K. Green, G. J. Flores, Rev. Sci. Instrum 70 Jan. 1999, to be published

15 P.W.J.M. Boumans: Indusctively coupled plasma, Emission spectroscopy, part 2, eds. Wiley interscience, 1987, chapter 10, 353.

16 G. Herzberg: Molecular spectra and molecular structure, spectra of diatomic molecules, part 1, eds. Van Nostrand Reinhold Company, 1950, chapter 3, 126.

17 K. Ogura, H. Yamada, Y. Sato, and Y. Okamoto: Applied Spectroscopy 51 No. 10, (1997), 1496.

18 W.L. Wiese and J.R. Furh: J. Chem. Ref. Data 4 (1975), 263.

19 CRC Handbook of Chemistry and Physics. David R. Lide Editor in Chief, 76th edition, 1995-1996.

20 J. Hermanus Maria: Measurements of optical excitation function of the mercury atom, Proefschrift-Utrecht publisher, 1961.

3. Observation of Self Absorption of Mercury and Cadmium Emission in an Atmospheric Microwave Sustained Plasma

Kamal Hadidi*, Paul Woskov, Karyn Green, Paul Thomas

3.1 Abstract

Atomic emission spectroscopy of a continuous, atmospheric-pressure microwave sustained plasma in an undiluted slip stream of stack exhaust is under development for real-time monitoring of EPA regulated hazardous metals (As, Be, Cd, Cr, Hg, and Pb). The detection limit in such a plasma for two of these metals on their strongest transitions, Cd I 228.8 nm and Hg I 253.65 nm, has been found to depend on the path length between the plasma and the detection system. Measurements were carried out on long plasma columns >100 mm x ~10 mm diameter sustained in air by approximately 1.5 kW power at 2.45 GHz. The detection limit using a long path-length axial view for UV light collection versus short path-length side views at different points along the plasma column have shown a clear diminution of the signal for the axial view. Self-absorption by unexcited atomic cadmium and mercury is shown to be responsible for diminution of the axial signal. The Cd I 228.8 nm transition was observed to reverse from an emission feature to an absorption feature when the axial path-length was increased.

3.2 Introduction

Because of public concern and the health problems they can cause, tougher regulations are being proposed for stack emissions of hazardous metals such as mercury, cadmium, and arsenic, which will require real time monitoring. Many industrial plants such as power plants, thermal processing plants and other industrial sources will need such monitors. Until recently, no continuous monitoring method for metals was available. In the USA, the Environmental Protection Agency (EPA) uses Method 29 for testing metals emissions compliance with clean air regulations. However, this method is not real-time, only providing a historical record of emissions. It requires the taking of a sample from the stack and having it analyzed in the laboratory. This process can take days before the results are known. To our knowledge, there is only one commercial real-time metals monitoring system available on the market[1]. Improvements are still needed in measurement accuracy, sensitivity, and affordability of continuous emission monitors (CEMs) for metals.

Several methods that make use of plasmas for atomic emission spectroscopy (AES) of trace metals are being developed as CEMs. Some of these methods such as inductively coupled plasma (ICP)[1, 3] and laser induced breakdown spark (LIBS) systems[4, 5] have limitations in one or more of the requirements for accuracy, sensitivity, and the capability for isokinetic sampling. A microwave plasma-based continuous monitor for real-time atomic emission spectroscopy of trace metals in stack exhaust[6] is being developed at MIT Plasma Science and Fusion Center. It can operate continuously in large volume, fast flowing stack exhaust with an attached metals injection system for span calibration.

* Corresponding author: hadidi@psfc.mit.edu

Excellent minimum detection limits and good accuracy have been achieved in air and undiluted stack exhaust for Pb, Be, and Cr[6,7]. Good detection limits have also been achieved for Cd, Hg, and As in pure nitrogen gas plasmas. However, the detection limit for Hg, Cd, and As has been found to degrade significantly in an air plasma[8]. It is important to understand the mechanisms by which the sensitivity for these metals is degraded in order to be able to further optimize this CEM for its intended application.

Previously we have shown that when oxygen is added to a nitrogen plasma, there is a significant reduction in the atomic emission of metals with high excitation energy levels such as mercury and arsenic[8]. Concurrent with the reduction in the metals UV emission, a slight lowering of the atomic excitation temperature was measured. No UV absorption was observed due to ozone or other molecular species in the plasma. Therefore, the effect of oxygen is to reduce the excitation of the atomic metals species in the plasma. Researchers of mercury arc plasmas have also noted a connection between temperature and emission intensity. The net radiative emission from a mercury arc lamp was observed to decreased by two orders of magnitude when the temperature of the plasma decreased from 6000 K to 4500 K[9]. It was concluded that self-absorption in the outer cooler regions of the plasma was needed to explain this result.

In this paper we present experimental measurements that support this argument for the microwave CEM plasma. Self-absorption of atomic emission is observed on strong metal transitions having their lower electronic level in the ground state. Both Cd I 228.8 nm and Hg I 253.65 nm are shown to have stronger self-absorption in plasmas with oxygen, supporting the previous claim that the addition of oxygen to the plasma reduces the atomic excitation of metals with high energy excitation states. The resulting increase in the population of unexcited atomic species causes an increase in UV absorption, compounding the problem of reduced emission of energetic transitions that terminate on the ground state.

3.3 Experimental Setup

The experimental setup, as described previously[8] was adapted for UV emission/absorption measurements as shown in Figure 3-1. A 1.5 kW, 2.45 GHz magnetron source irradiated a gas flow in a dielectric tube (25.4 mm i.d.) transversing a shorted WR-284 (72 x 34 mm) waveguide. The plasma flame was approximately 10 mm in diameter and extended for more than 100 mm from the center of the waveguide. Four slits 10 mm in length and 2 mm wide were cut into the side of the waveguide and in the after glow channel along the plasma column in order to view the plasma from the side, perpendicular to the plasma axis. A detail of these silts is shown in Figure 3-2. The slits were covered with quartz plates and sealed with RTV in order to prevent air leaks into the

plasma. The boron nitride tube used in previous experiments[8] was replaced with a quartz tube in order to view the plasma from the side.
The side viewing UV light collection optics consisted of a 5 mm diameter, ~10 mm focal length lens positioned on the quartz plate at the center of a slit. The lens focused the light onto a 0.8 mm core fiber optic cable positioned at the focal point. The side viewing optic system was moved from slit to slit for the measurements that are presented here.

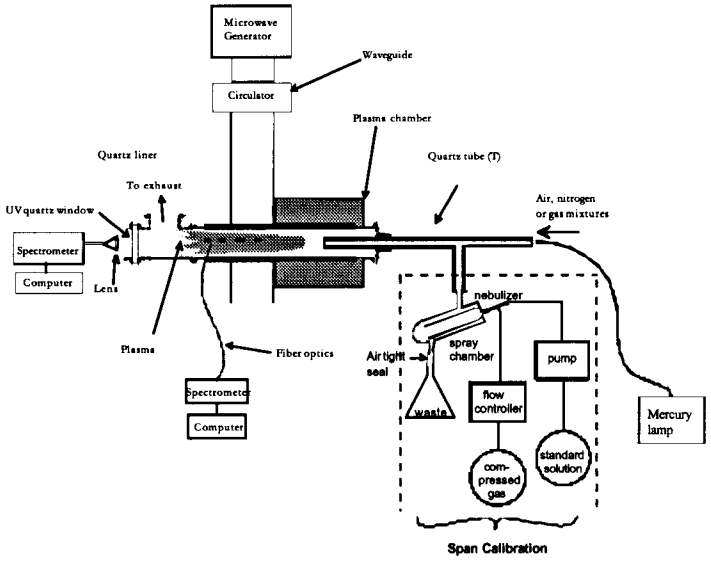

Figure 3-1. Experimental setup

For most of the experiments, the axial view of the plasma was performed at a distance of 25 cm from the waveguide. The light was collected through a 50 mm diameter quartz window and lens that focused it onto a 0.8 mm core fiber optic cable at a focal length of 75 mm. This optical system was mounted on the axial branch of the plasma exhaust tubing steel Tee (internal i.d. 38 mm) used to connect the exhaust pump to the side. The center of the perpendicular branch of the Tee was 11 cm from the waveguide. For some experiments with cadmium, and to study the effect of a longer path length on emission and absorption, we used a longer Tee. For this Tee, the distance between the waveguide and the optical system was 36 cm, and the distance between the waveguide and the exhaust was 21 cm.

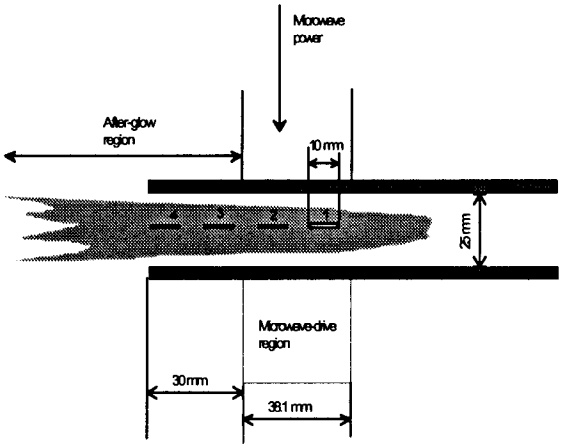

Figure 3-2. Details of the side measurement setup

The fiber optic cable, which was 2 m long for both side and axial view, was connected to a 0.64 m grating spectrometer with a Princeton Instruments 512-element linear detector array. For each measurement, a set of background spectra was taken first, using clean deionized water, then an aerosol of the desired element was injected and another set of spectra was taken. The aerosol contained either mercury or cadmium at 10,000 μg/ml in a 5% HNO_3 solution. It was assumed that the clean water background was representative of the dilute water/HNO_3 acid background spectrum. The aerosol injection, calibration

system, and the calculation method for the metals concentration in the gas flow were described previously[8].

The base plasma gas flow rates were14 liter per minute of air for the axial sample line flow and 9 l/min nitrogen for the swirl flow, which confined the plasma to the center of the discharge tube. The integration time for data acquisition was 0.1 second and 3 minute data sets of 600 sequential spectra were recorded of each background and metal signal. The first step in the data analysis involved the identification of the relevant detector pixels for a given metal transition and plotting the signal of those pixels as a function of time. The next step consisted of smoothing out the background and the signal over 10 points and then subtracting the background from the metal signal. The results were further averaged for an integration time of 1 min.

The minimum detection limit (MDL) is calculated as 3 times the standard deviation of the signal fluctuations. In units of $\mu g/m^3$ it is given by the following formula:

$$MDL = 3\frac{\sigma}{S}C_{span} \qquad (3\text{-}1)$$

where σ is the standard deviation of the signal fluctuations, S is the signal intensity in the same units as the standard deviation, and C_{span} is the concentration of the metal in $\mu g/m^3$ that produces signal S. In our system a pneumatic nebulizer is used to inject a known metals concentration into the plasma and C_{span} is given by:

$$C_{span} = \frac{\varepsilon XR}{F} \qquad (3\text{-}2)$$

Where ε is the nebulizer efficiency for metals transport, X is the standard solution concentration in $\mu g/ml$, R is the rate of solution in ml/min pumped into the nebulizer, and F is the volume flow rate of gas in the sample line in m^3/min. The Meinhard Type A pneumatic nebulizer used for this work had a measured metals transport efficiency of 0.9% and the solution uptake rate was nominally 1 ml/min.

3.4 Results

Most atomic emission from the microwave plasma is optically thin. Consequently, the longer the path length in the plasma for UV/light collection the higher the emission signal. For this reason the axial optics viewing geometry provides the strongest signals and the lowest detection limits for most metals. In our present setup this includes the strong atomic emission of lead, chromium, and iron. However, in a few important cases the opposite is true. This includes the primary transitions used for monitoring cadmium and mercury.

Figures 3-3 and 3-4 show the measured minimum detection limit (MDL) and standard deviation for Cd I 228.8 nm and Hg I 253.65 nm lines, respectively. The plots are a function of the different light collection views, the four side views from the waveguide

out to the afterglow and the axial view. The MDL is lowest for the side views. For Cd I 228.8 nm the MDL is at its minimum at side 2 where it reaches 38 μg/m^3 and increases sharply for axial viewing to 1292 μg/m^3. For the Hg I 253.65 nm the MDL also reaches its minimum at side 2 at 73 μg/m^3 then increases to a maximum at side 4 of 128 μg/m^3. It decreases to 91 μg/m^3 for the axial view, but is still higher than the best side view limit.

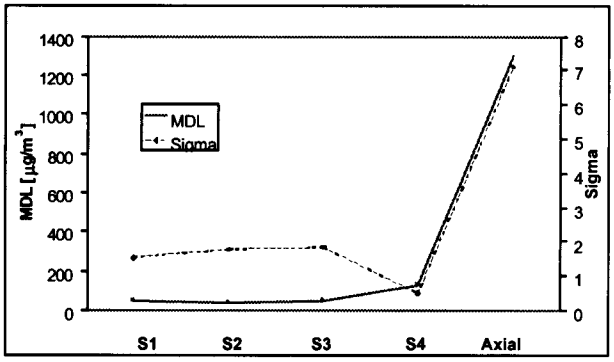

Figure 3-3. Minimum detection limit (MDL) and standard deviation (sigma) for Cd I 228.8 nm

The standard deviation of the signal fluctuations are also low for the side views for both these transitions and then increase to a maximum for the axial view. This increase in the standard deviation more than offsets stronger axial signals to make the axial view MDL higher as calculated by equation (1). Both these cadmium and mercury transitions terminate on ground states making them susceptible to absorption by unexcited cadmium and mercury atoms. However, the fact that a transition terminates on a ground state is not sufficient by itself to cause a transition to have a higher detection limit for the longer path-length axial view.

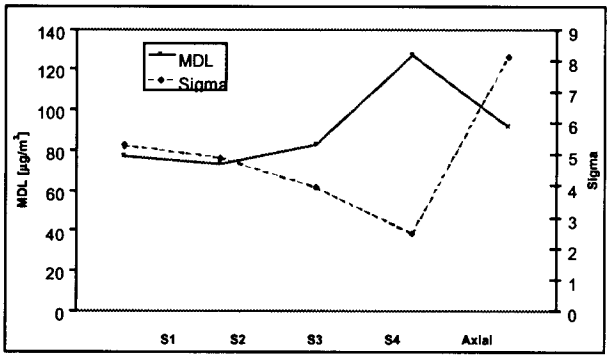

Figure 3-4. Minimum detection limit (MDL) and standard deviation (sigma) for Hg I 253.65 nm

This is demonstrated by measurements taken on the Cd I 326.1 nm line, also a ground state terminating transition, shown in Figure 5. As can be seen, the MDL for this line decreases from 166 μg/m^3 for side 1, to 68 μg/m^3 for side 2. It increases again for side 3 and side 4 to reach 132 μg/m^3, then it dramatically decreases to reach a minimum at 8 μg/m^3 for the axial view.

The low axial MDL for the Cd I 326.1 nm transition is due primarily to a significant increase in UV signal levels when the collection optics view axially, as is the case for most axial atomic emission. The MDL is a minimum despite a maximum for the axial signal standard deviation. Figure 3-5 shows that the standard deviation stays approximately constant at a low value from side 1 to side 4 and then increases sharply for the axial view. The increase in axially collected UV emission levels more than compensates for this increase in signal fluctuations to result in a low MDL as calculated by equation (1).

The sharp increase in the standard deviation of the axial viewed signal for all atomic emission suggests that turbulence in the plasma afterglow could be an important mechanism suppressing the MDL. Turbulence is present because the exhaust flow must make a sharp 90° bend 11-cm from the waveguide.

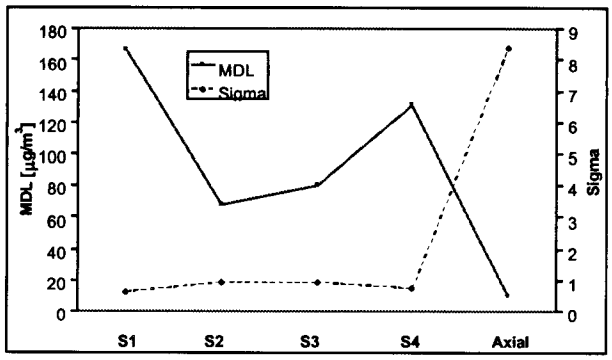

Figure 3-5. Minimum detection limit (MDL) and standard deviation (sigma) for Cd I 326.1 nm

An extension was added to the exhaust Tee to move this turbulent region further away (21 cm) from the waveguide and plasma UV emission region. The resulting axial spectra for this longer axial path length clearly showed that self-absorption by unexcited atoms is the dominate mechanism for reducing the MDL of Cd I 228.8 nm and Hg I 253.65 nm.

Figure 3-6 shows spectra of Cd I 228.8 nm and Cd II 226.5 nm. In figure 6a the emission spectrum is for the shorter axial length and shows the two cadmium transitions in emission. In figure 6b the axial length is 11 cm longer and the Cd I 228.8 nm transition reverses into an absorption feature. There is no change in the Cd II 226.5 emission because this line is not absorbed by unexcited atomic cadmium. Similar spectra for Hg I 253.65 nm emission did not produce an absorption feature, but the emission level on this line was significantly reduced for the longer axial path length.

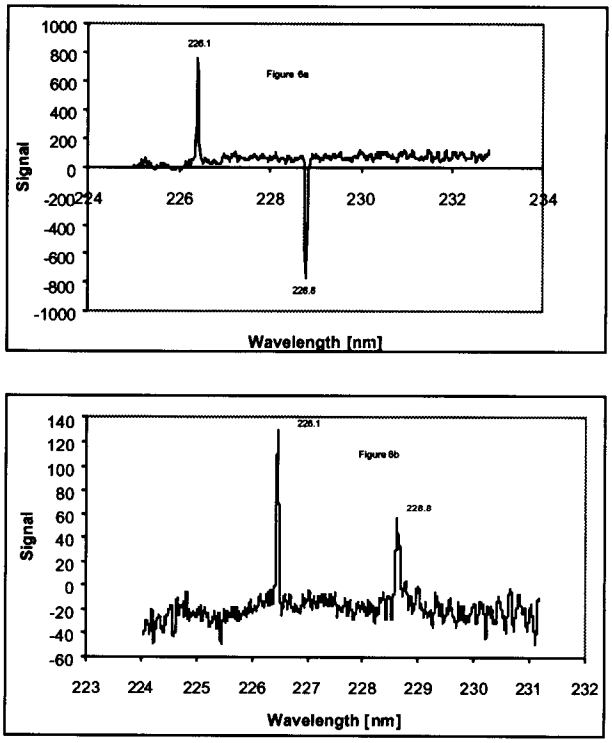

Figure 3-6b. Spectra of Cd I 228.8 nm and Cd II 226.5 nm a) the emission spectrum is for the shorter axial length and shows the two cadmium transitions in emission. In figure 6b the axial length is 11 cm longer and the Cd I 228.8 nm transition reverses into an absorption feature.

3.5 Discussion

The Cd I 228.8 nm emission is a $5p(^1P^o_1) \rightarrow 5s^2(^1S_o)$ transition with an excitation energy of 5.42 eV and the Hg I 253.65 nm emission is a $6p(^3P^o_1) \rightarrow 6s^2(^1S_o)$ transition with an excitation energy of 4.89 eV. The mercury transition is a forbidden transition, violating the selection rule against singlet-triplet transitions. Consequently, this mercury transition has a weaker absorption oscillator strength (0.0245) [10] than the Cd I 228.8 nm transition (1.4). This would explain the higher degree of self-absorption observed on the cadmium line. Also the high excitation energy would explain why the optimum side-viewing region for these transitions is at side 2. It is here that the metals aerosol has had the longest residence time in the plasma to be volatilized while still being in the waveguide. The high microwave electric fields in the waveguide generate the energetic electrons that excite these transitions. The energetic electrons would be quickly collisionaly quenched up stream of the waveguide and therefore excitation of these energetic states would not be as efficient outside the waveguide.

The Cd I 326.1 nm emission is a $5p(^3P^o_1) \rightarrow 5s^2(^1S_o)$ transition with an excitation energy of 3.80 eV. This cadmium transition is the same singlet-triplet transition as the Hg I 253.65 nm transition but at electronic level 5 instead of 6. Therefore, this is also a forbidden transition, but in this case the selection rule against singlet-triplet transitions holds more strongly. The absorption oscillator strength of Cd I 326.1 nm (0.0019) is three orders of magnitude weaker than that for the Cd I 228.8 nm transition and over an order of magnitude weaker than the Hg I 253.65 nm transition. This would account for the lack of observing self-absorption for this longer wavelength cadmium transition.

The observed diminution of the detection limit for mercury and cadmium (on the 228.8 nm transition) in an air plasma is the combination of three effects. First, oxygen in the air reduces the excitation of the energetic metal transitions creating a higher population of unexcited atomic species. The second effect is then absorption by these unexcited atoms that further reduces emission due to the weaker atomic excitation. The third effect is the increased signal fluctuations due to combined fluctuations in both absorption and emission. According to equation (1) the MDL is not only inversely effected by signal strength, but is also proportional to signal noise.

The experimental measurements presented here show that the absorption becomes stronger with increased light collection path length through the plasma, particularly axially through the afterglow region where the population of unexcited atoms would be at a maximum. The extreme case being that shown in figure 6b when the path length is long enough to reverse an atomic emission feature into an atomic absorption feature. Even for short paths through the side of the plasma self-absorption would effect the signals because of a gradient in the temperature distribution due to the swirl flow, which keeps the plasma from attaching to the dielectric walls. However the self-absorption would be kept to a minimum due to the short path length.

Another advantage of the side view is a more stable plasma. The increased self-absorption along the axial view is aggravated by viewing through the most turbulent gas

flow region in the afterglow or beyond where the plasma exhaust makes a sharp turn. Such a diversion of the exhaust flow is necessary to provide axial viewing access. The absorbing species in the turbulent region greatly increases the signal fluctuations from a more stable emission region behind the turbulent region. We briefly examined the possibility of monitoring cadmium using the Cd I 228.8 nm line in absorption and found the detection limit to be much higher than viewing this transition in emission from the side.

3.6 Conclusion

The development of a multi-metal CEM for stack emissions using atomic emission spectroscopy requires operation with non-ideal plasma conditions to insure accurate sampling of the stack exhaust. Unlike laboratory ICPs and microwave induced plasmas where a noble gas matrix and flow rate are carefully controlled to achieve maximum sensitivity, a stack mounted CEM must operate with a molecular gas matrix such as air and at high velocity gas flow rates to achieve isokinetic sampling for accuracy. The atmospheric microwave sustained plasma has been shown to be very good at stable operation under such conditions. It can operate continuously in larger volumes and faster flows with lower power than any other stack plasma excitation method demonstrated to date. However, in order to best exploit this capability for application to metals monitoring it is necessary to better understand the details of the plasma atomic emission process under a wider ranged of plasma conditions. This would be true for any *in situ* plasma excitation method.

In the study presented here it has been shown that self-absorption of atomic emission lines occurs in a microwave-sustained air plasma for mercury at 253.65 nm and cadmium at 228.8 nm. Consequently, when picking emission transitions to monitor metals and setting up the UV light collection optics self-absorption must be considered. In the case of cadmium a line other than Cd I 228.8 nm without a strong absorption oscillator strength can be used for monitoring. For mercury, where another strong emission line for monitoring is not available, we need to locate the UV collection optics where the Hg I 253.65 nm excitation is a maximum and minimize the UV light propagation path length through regions having unexcited atomic mercury. This requires locating the UV collection optics as near as possible to the microwave driven region. With appropriate design, atmospheric microwave-sustained plasma should be capable of monitoring all hazardous metals simultaneously for insuring compliance of stack emissions with EPA regulations.

3.7 References

1 G. A. Meyer, Proceedings of SPIE, Vol. 3534, Environmental Monitoring and Remediation Technologies, Boston, Nov. 1998, 677.

2 C. Trassy, R. Diemiaszonek, P. Pasquini, and R. Meunier: Proc. of Int. Sym. on Environmental Technologies, Plasma System and Applications, Atlanta, 1995, 401.

3 M. D. Seltzer and R. B. Green: Process Control and Quality. 1994, **6** No. 1, 37.

4 D. W. Hahn: Appl. Phys. Lett. 1998, **72**, 2960.

5 J. P. Singh, Fang-Yu Yueh, Hansheng Zhang, R.L. Cook: Process Control and Quanlity 1997, **10**, 247.

6 P. P. Woskov, K. Hadidi, P. Thomas, K. Green, and G. J. Flores, Univ. Calif. Irvine, Proceedings of the IT3 Conference, Session 15, Orlando, USA, May, 1999. www.psfc.mit.edu/library/99ja/99ja011/99ja011_abs.html

7 P.P. Woskov, K. Hadidi, P. Thomas, K. Green, G. Flores, and D. Lamar: Massachusetts Institute of Technology, PSFC/RR-98-1, 1998. www.psfc.mit.edu/library/98rr/98rr001_abs.html

8 K. Hadidi, P.P. Woskov, G.J. Flores, K. Green, P. Thomas: Japaneese Journal of Applied Physics No.7B, Vol.38 (1999) Special issue : Plasma Processing.

9 R.J Zollweg. J. Appl. Phys. 1978, **49**, 3,

10 A. A. Radzig and B. M. Smirnov, Reference Data on Atoms, Molecules and Ions, Chap. 7, Springer-Verlag, Berlin, 1985.

4. Electronic Excitation Temperature Profiles in an Air Microwave Plasma Torch

K.M. Green, M.C. Borrás, P.P. Woskov, G.J. Flores III, K. Hadidi, P. Thomas

Plasma Science and Fusion Center, Massachusetts Institute of Technology, 167 Albany Street, Cambridge, MA 02139

4.1 Abstract

A 0.9 to 1.5 kW, 2.45 GHz atmospheric pressure air microwave plasma torch has been operated efficiently with less than 1 % reflected power. The plasma is sustained in a 28 mm internal diameter fused quartz tube which penetrates perpendicularly through the wide walls of a tapered and shorted WR-284 (72 x 17 mm cross-section) waveguide. A study has been made of the effects of power and airflow on the electronic excitation temperature, T_{exc}. Abel inversion of radial profile chord averaged Fe I emission lines in the 370 to 377 nm range have been used to obtain localized profile measurements of T_{exc} inside the waveguide excitation region. In general, temperature profiles peak on axis with no evidence of a skin effect in the large diameter (10 mm FWHM emission intensity) plasmas. A maximum central T_{exc} of 6550 K ± 350 K is observed at an airflow rate of 28 lpm. When maintaining a constant flow rate of 14 lpm, a 55 % increase in microwave power from 0.9 to 1.4 kW causes a ~100 % increase in plasma volume without any noticeable effect on the central T_{exc} value. At a constant microwave power of 1.4 kW, an increase in total flow rate from 11 to 28 lpm decreases the volume of the plasma by ~25 % and increases the central T_{exc} by ~13 %. The axially peaked temperature profiles are consistent with an electron density of ~ 10^{13} cm^{-3}.

Index terms: electronic excitation temperature, microwave plasma, atmospheric pressure plasma, atomic emission spectroscopy

4.2 Introduction

Considerable interest exists in medium to high-power, atmospheric pressure microwave sustained plasmas for environmental and industrial processing as well as monitoring applications. The main advantages of such plasmas are electrodeless operation, high throughput atmospheric processing, efficient microwave to plasma coupling, and availability of inexpensive sources at 0.915 and 2.45 GHz. Low power (< 500 W) atmospheric pressure microwave-induced plasmas (MIPs) have had a long history of use for laboratory spectroscopic analysis instrumentation. Such plasmas can be formed in resonant cavity, waveguide, or surface-effect systems [1]. The plasma gas typically consists of argon, helium, nitrogen, or air [1]-[4]. More recently, there have been studies and applications of higher power (>1 kW) microwave plasmas to increase plasma robustness for laboratory spectroscopic analysis [5, 6], continuous emissions monitoring in the field [7], commercial processing [8], and other applications [9].

Atmospheric microwave plasmas can operate over a wide range of electron plasma density regimes from low density glow-discharge like plasmas [8, 9] to higher density arc-discharge like torch plasmas [5-7]. The work reported here focuses on a microwave plasma torch (MPT) under development for continuous emissions monitoring of smokestack hazardous metals air pollution. The MPT can be a reliable stack mounted technology for real-time atomic emission spectroscopy of trace metals [7]. However, the excitation efficiency in an air plasma for some metals with high electronic excitation energies is not as high as in a plasma without oxygen in the gas matrix [10,11]. Understanding how the electronic excitation temperature may be increased in an atmospheric air MPT would be of value for reducing the detection limits for some important pollutants such as mercury and arsenic.

Atmospheric pressure microwave plasmas are not as well studied as radio frequency inductively coupled plasma (ICP) systems. Numerous plasma temperature studies have been performed of ICPs. In these studies the temperature is lower in air plasmas, which impedes the excitation of the sample species and, therefore, depresses the characteristic atomic line emission. Gomes et al. [12] report lower temperatures in air ICP plasmas than in argon ICP plasmas, explaining that the polyatomic species in air store energy in their excited levels. Abdallah and Mermet [13] report that a few percent of nitrogen introduced into an argon ICP plasma also reduces the plasma temperature. In the case of a MPT, Hadidi et al. [10] have shown that the addition of oxygen to a nitrogen plasma decreases the rotational and electronic excitation temperatures. Since the presence of molecular species is inherent to an air MPT for application as a stack pollution monitor, the objective of the experiments reported here is to examine the effect of other parameters such as microwave power level and volume of gas flow on the electronic excitation temperature.

4.3 Experimental Setup

The experimental setup used is shown in Figure 4-1. The microwave generator is an ASTeX Model S-1500i 1.5 kW, 2.45 GHz magnetron source. The output of the

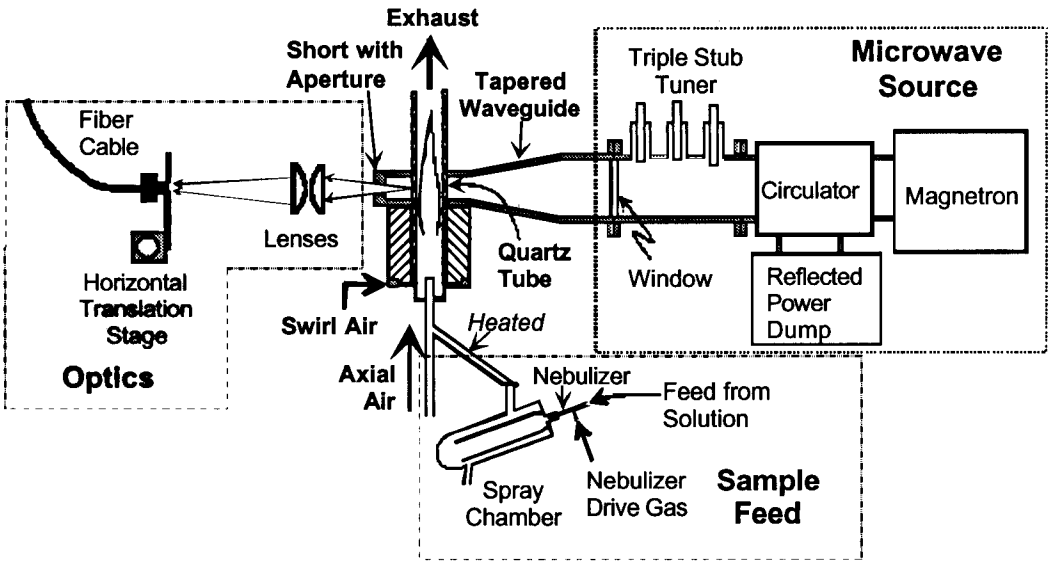

Figure 4-1. Experimental setup of the microwave plasma torch for atomic emission profile measurements.

magnetron is connected by WR-284 waveguide to a circulator, which in turn is connected to a triple stub impedance matching tuner and a water-cooled reflected power dump. A Teflon window seals the output of the triple stub tuner to keep the circulator and magnetron clean of dust from the plasma end of the waveguide. Microwave detectors at the magnetron input to the circulator and at the circulator output to the dump continuously monitor forward and reflected power. During the present experiments, the forward microwave power is varied over the range of 0.9 kW to 1.4 kW. The reflected power can be adjusted with the triple stub tuner to less than 1 % of the forward power. Even with all the tuning stubs completely withdrawn reflected power is typically less than 10%.

The plasma is sustained by the microwaves in a tapered and shorted waveguide attached to the windowed end of the triple stub tuner. The cross-section of the waveguide at the tapered plasma end is 72 x 17 mm. The plasma gas flow is confined inside a quartz tube with a 32 mm outside diameter and a 2 mm thick wall. This quartz tube penetrates through the center of the wide waveguide walls one-quarter (30.6 mm) waveguide wavelength back from the short where the E-field is peaked before the plasma is started. There is no resonator structure. Once the plasma is started the microwaves are beamed directly into the absorbing plasma without obstruction. The plasma is started with a small tungsten Hertz spark loop on the tip of an alumina rod, which is briefly inserted into the quartz tube in the waveguide.

Tangentially injected swirl airflow into the quartz tube upstream of the waveguide keeps the plasma off the inside walls of the quartz, confining the plasma to the center of the tube. An axial airflow transports the sample to be atomized and excited by the plasma for

spectroscopic study. The swirl and the axial airflows typically each make up half of the total gas flow through the plasma. A branch in the axial airflow line connects to a sample feed source. The sample feed source consists of a pneumatic nebulizer and a spray chamber. The nebulizer aerosolizes a weak acid solution containing the element to be studied and ejects the mist into a spray chamber at a rate of ~1 ml/min each for the liquid and drive gas feed rates. The spray chamber limits water loading by filtering large droplets (over 99 % of the original solution) into a waste container [14]. The branch line is heated to volatilize the liquid droplets as they are transported to the plasma.

The plasma emission light is viewed through a large aperture in the waveguide short. The aperture is beyond the cut off for transmission of 2.45 GHz radiation with a cross-section of 32 x 12.7 mm and a depth of 30 mm. A pair of quartz lenses image and magnify, by a factor of two, the plasma light onto a plane where a fiber optic cable is used to scan the plasma diameter. The fiber optic is a UV quartz cable with a core diameter of 0.8 mm and a numerical aperture of 0.22. Data collection occurs for up to sixty-six chords that are evenly spaced in one-millimeter increments.

The fiber optic is connected to an Instruments S.A. Model THR-640, 0.64 m spectrometer which has a 2400 groove/mm grating, an adjustable slit, and a Princeton Instruments Model IRY-512W intensified 512-element detector array. For the present experiments with atomic iron emission, this spectrometer is tuned to cover the 370 – 377 nm spectral range with a spectral resolution of about 0.05 nm.

The sample feed uses an Alpha Aesar calibrated solution having a concentration of 10,000 μg/ml of iron dissolved in a 5% solution of nitric acid. To obtain accurate emission levels when the aerosol iron sample is injected into the plasma, deionized water is first injected to obtain a blank water background spectrum. Subtracting the water background from the iron spectrum removes the influence of the water loading on the plasma light intensity. The influence of the nitric acid on the plasma is assumed negligible, and all remaining signal light is assumed due only to the influence of the iron in the plasma. Figure 4-2 shows a representative iron spectrum obtained in the present setup.

4.4 Theory

4.4.1 Abel Inversion

The Abel inversion allows for the transformation of line-integrated data to localized values [15]. In the case of the microwave plasma torch, the Abel inversion technique permits transforming the line-integrated plasma light intensity, $I(y)$, into the localized radial emissivity, $\varepsilon(r)$. Figure 4-3 illustrates the analytical geometry and defines some of the parameters. The line-integrated intensity and the radial emissivity are respectively given by [16]

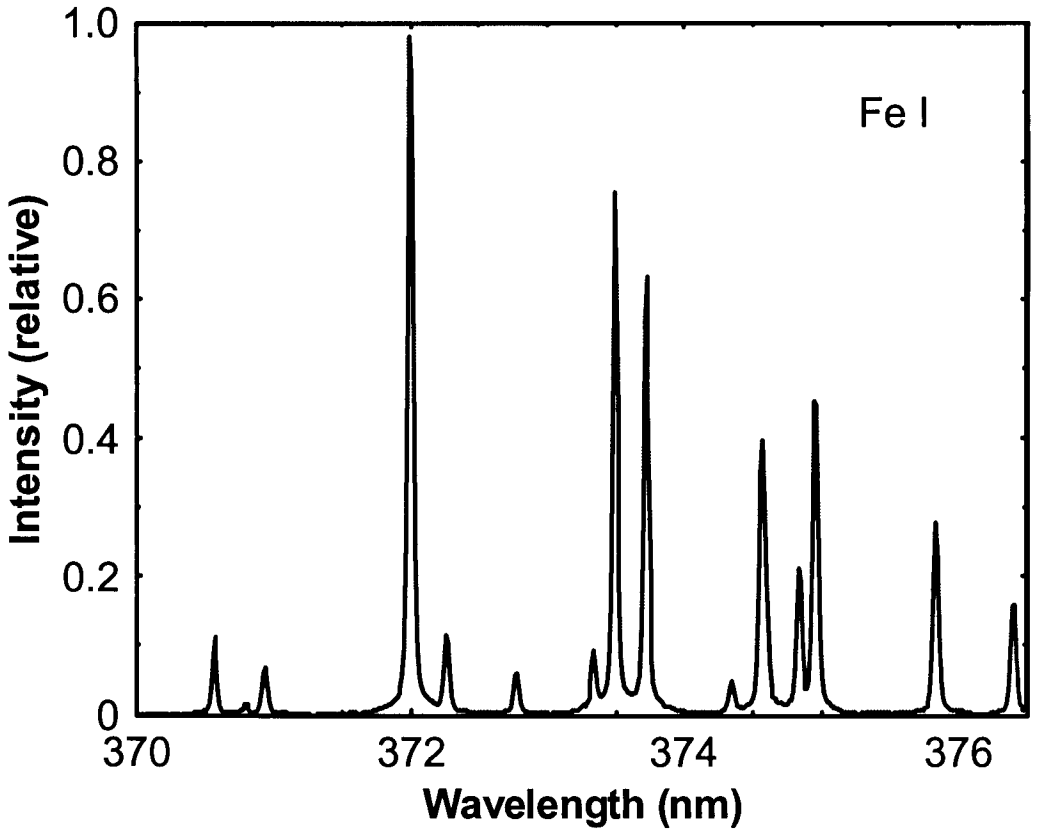

Figure 4-2. Typical atomic iron (Fe I) spectrum observed in the MPT.

$$I(y) = 2\int_{y}^{R} \frac{\varepsilon(r)}{\sqrt{r^2 - y^2}} r dr \tag{4-1}$$

$$\varepsilon(r) = -\frac{1}{\pi}\int_{r}^{R} \frac{\frac{dI(y)}{dy}}{\sqrt{y^2 - r^2}} dy \tag{4-2}$$

where R is the maximum plasma radius. The units for the line integrated intensity and for the radial emissivity are $Wm^{-3}sr^{-1}$ and $Wm^{-4}sr^{-1}$, respectively.

The Abel inversion technique requires a symmetric intensity function as well as the necessity for the intensity to fall to zero at the plasma edge [17]. To ensure that these specifications are met, a subtracted Gaussian is fit to the intensity profile data of each iron line. This curve has the form

$$I(y) = Ae^{-by^2} - Ae^{-bR^2} \tag{4-3}$$

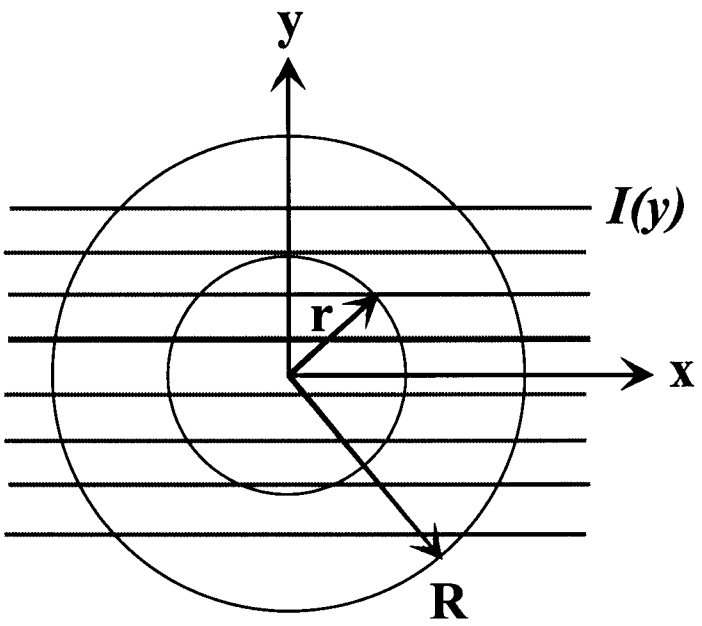

Figure 4-3. Geometry for Abel inversion.

where A and b are fitting parameters unique to each intensity profile. Each iron line is inverted using Equation 4-2 to obtain the derived radially localized emissivity

$$\varepsilon(r) = \frac{1}{\sqrt{\pi}} A b^{\frac{1}{2}} e^{-br^2} erf\left(\left[b\left(R^2 - r^2\right)\right]^{\frac{1}{2}}\right) \tag{4-4}$$

where r is the radial parameter.

4.4.2 Determination of T_{exc}

The excitation temperature, T_{exc}, is determined by fitting a thermal distribution to the appropriately weighted intensities of a set of atomic transitions for a specific atomic species in the plasma [18]. In the case of the MPT experiments, the atomic species used is iron. The localized intensities, I_{ij}, of neutral atomic iron, Fe I, transitions are the quantities obtained by the Abel inversion of the measured chord averaged intensities in the MPT system. The iron lines of interest fall in the range between 368 nm to 377 nm. To yield T_{exc}, the appropriate statistics and oscillator strengths are used to scale the intensities. Each observed Fe I wavelength has an associated energy level, E_j, a statistical weight, g_i, and oscillator strength, f_{ij}, as given in Table I [19]. The calculation of T_{exc} at a particular radius entails plotting $\log(I_{ij}\lambda^3 / g_i f_{ij})$ versus E_j [18]. The slope of a straight line fit to these points relates to the electronic excitation temperature by

$$T_{exc} = -\frac{0.625}{m} \tag{4-5}$$

where T_{exc} is in K, and m is the slope of the line [15]. The deviation from a straight line determines the error in T_{exc}.

Performing this calculation at each radial point provides the T_{exc} profile in the plasma. Since the light emission levels decline rapidly near $r = 10\ mm$, the error in T_{exc} becomes quite large beyond this range. Therefore, the T_{exc} profile measurements extend only to this radius.

A key assumption in this analysis of T_{exc} is that neutral atomic iron and the electrons are each in thermal equilibrium. If the plasma is shown to be in or near local thermodynamic equilibrium (LTE), then this assumption is valid. The condition of LTE specifies that all temperatures in the plasma are equal except the blackbody radiation temperature [15]. LTE requires that the collisional processes dominate the radiative processes in the plasma [17].

Table I. Fe I Emission Lines Used for T_{exc} Determination [19]

Wavelength, λ (nm)	E_i (cm^{-1})	$10^{20}\lambda/gf$ (m^3)
368.222	55754	2.6202
368.411	49135	9.5279
370.108	51192	5.1878
370.446	48703	18.8875
371.993	26875	13.8549
372.438	45221	25.8918
372.762	34547	17.1512
373.239	44512	16.4422
373.486	33695	2.5517
373.713	27167	19.3916
374.826	27560	53.8876
374.948	34040	3.5638
375.823	34329	5.3082
376.379	34547	8.258
376.554	52655	1.5757
376.719	34692	11.6964

4.4.3 Determining Proximity to LTE

Griem [20] has established a criterion for the determination of a plasma's proximity to LTE. This formulation places a lower limit on the electron density. The Griem criterion states

$$n_e \geq 9\times10^{11}\left(\frac{\Delta E}{E_H}\right)^3\sqrt{\frac{T_e}{E_H}} \tag{4-6}$$

where n_e is the electron density in cm^{-3}, ΔE is the energy level difference between the ground state and the first ionization state, E_H is the ionization potential for hydrogen (13.6 eV), and T_e is the electron temperature. Equation 4-6 is valid only for optically thin plasmas.

Evaluation of the Griem criterion necessitates knowledge of the electron temperature, T_e and density, n_e. Neither of these parameters could be directly measured in the present experiment, but a number of past results in atmospheric microwave plasmas can be used to estimate these values. Potts *et al.* [8] and Brandenburg *et al.* [9] have measured T_e of 1.1 and 0.67 eV, respectively, and have measured a n_e of ~ 7 x 10^{10} cm^{-3} in spatially extended ball lightning like microwave plasmas. In a more dense microwave torch plasma, Ogura et al [6] have measured a n_e of ~ 3 x 10^{13} cm^{-3} at 1 kW microwave power level in atmospheric pressure nitrogen. Timofeev [21] has also developed an electron density expression based on experimental data from an atmospheric pressure spherically symmetric microwave air discharge. The electron density is given by

$$n_e = \begin{cases} 5.91\times10^{15} e^{\frac{14.42}{T-1.74}} & (T>1.74) \\ 0 & (T<1.74) \end{cases} \tag{4-7}$$

where n_e is in cm^{-3}, and T is the temperature at LTE measured in 10^3 K. Anticipating our temperature measurements below, Equation 7 results in n_e of ~ 2 x 10^{14} cm^{-3}.

Evaluating Equation 4-6 for an electron temperature of approximately 1 eV and for a ΔE corresponding to the ionization potential for the N_2 molecule (15.6 eV) results in an electron density threshold of ~3 x 10^{11} cm^{-3} for LTE. This value is well below the electron densities for an atmospheric microwave torch plasma and near the measured values for the more tenuous ball lightning like microwave plasmas. Therefore, based on the Griem criteria the assumption of LTE is believed to be valid for the MPT T_{exc} analysis presented here. Further support for the validity of this assumption can be found in Borrás [22] where measurements of the rotational temperature in the present MPT system in nitrogen are presented and are approximately the same as the T_{exc} measurements presented below.

4.5 Experimental Results

4.5.1 As a Function of Microwave Power

For the experiments at different forward microwave power levels, the total airflow rate is held constant at 14 lpm. The data are collected at three power levels, 900 W, 1150 W,

and 1400 W. Figure 4-4 shows one of the chord averaged emission intensity profiles for the 373.5 nm Fe I transition at 1400 kW. The points represent experimental measurements, and the line is a best fit of Equation 4-3. The agreement between the subtracted Gaussian profile and the experiment is good. This profile is typical for other iron transitions and other power levels. Though all the measured profiles have a similar shape to that of Figure 4-4, the light emission intensity diameter and level increase with microwave power over the studied power range.

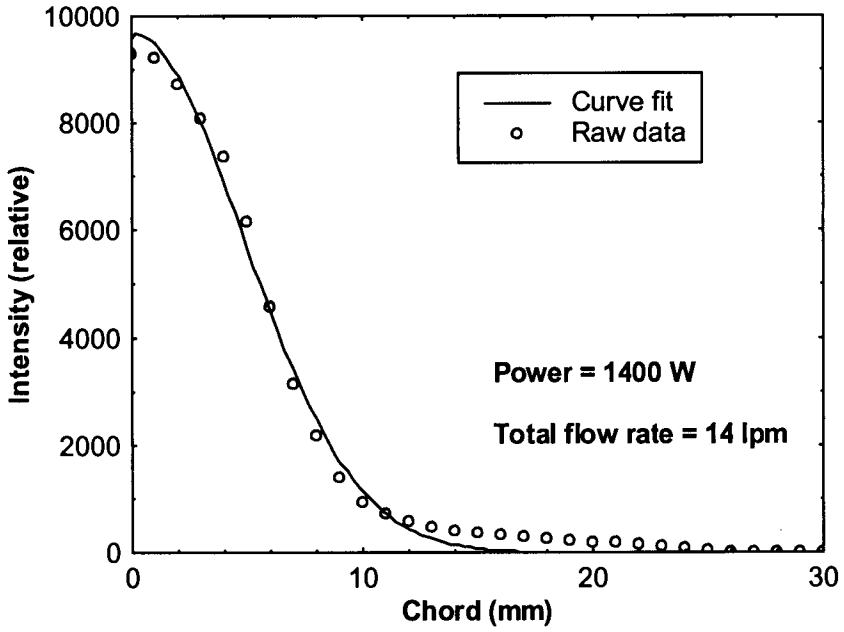

Figure 4-4. Radial profile of the chord averaged plasma emission intensity at the 373.5 nm Fe I transition. Points are experimental measurements and the line is a fit of Eq. 4-3.

Figure 4-5 depicts the Abel inverted and normalized light emission profiles for a representative Fe I transition. Quite noticeable is the increase in plasma size. The Abel inverted light emission intensity profiles are also well represented by Gaussian profiles peaked on axis, as expected. No evidence of profile flattening or going over to a hollow profile with increasing microwave power is observed to suggest a finite microwave absorption depth less than the maximum plasma radius.

As the forward microwave power is increased by 55 % from 900 W to 1400 W, the plasma diameter full width at half maximum (FWHM) increases from 4.5 to 6.5 mm. This growth corresponds to an increase in the plasma cross-sectional area and volume inside the waveguide by over 100 %. This observation is consistent with other RF driven atmospheric plasmas. Abdallah and Mermet [23] report an inflation in their inductively-coupled argon plasma with an increase in power.

Using the localized emission intensities of 12 or more Fe I transitions such as the one shown in Figure 4-5, a T_{exc} temperature fit is obtained as described in Section 4.3.2. A

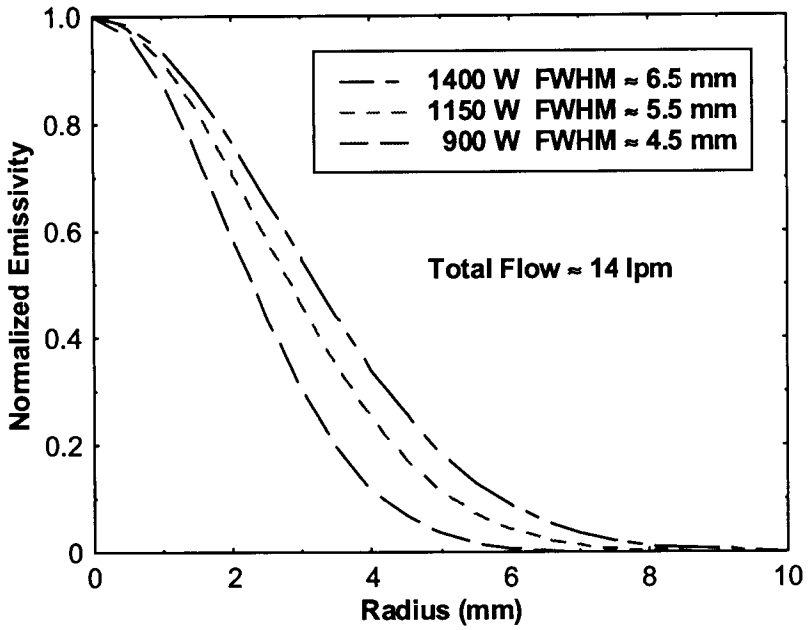

Figure 4-5. Normalized light emission at constant flow rate with varying power for a representative Fe I transition.

representative temperature fit is shown in Figure 4-6 for the axial temperature at 1400 W. Temperature fits such as this are done at each radial position across the scanned plasma radius. The emission light levels where strong enough on the weak Fe lines only out to a plasma radius of 10 mm to do a temperature fit. The resulting T_{exc} temperature profiles are shown in Figure 4-7. The temperature profiles are almost flat out to the largest measurable plasma radius of 10 mm with a maximum of 5800 K ± 200 K on axis. At the 10 mm radius this temperature is still 80% of its value on axis, where the plasma emission intensity is less than a few percent of its on axis value. Increasing the microwave power has no effect within the error bars of the measurements on the temperature of the plasma. This observation is consistent with other atmospheric microwave plasma work. Timofeev has reported that increasing the microwave power by two orders of magnitude produces only a minor effect on the plasma temperature of an atmospheric pressure microwave plasma discharge and flat profiles within a spherical discharge [21]. The additional microwave power contributes to expanding the plasma volume rather than heating the plasma to a higher temperature.

4.5.2 As a Function of Airflow

For the experiments at different airflow rates, the forward microwave power is held constant at 1400 W. Four total airflow rates, 11 lpm, 14 lpm, 23 lpm, and 28 lpm, are examined. For the 14 lpm case, the axial airflow constitutes 8 lpm while the swirl airflow makes up 6 lpm of the total flow. For all of the other airflow rates, the axial and swirl airflows constitute equal portions of the total.

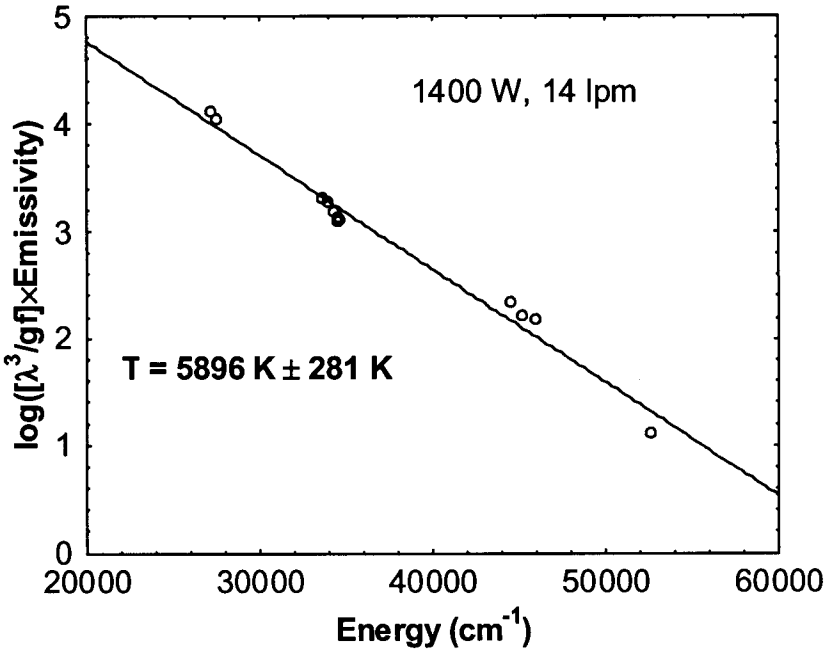

Figure 4-6. Temperature fit to localized iron transition emission intensities on axis.

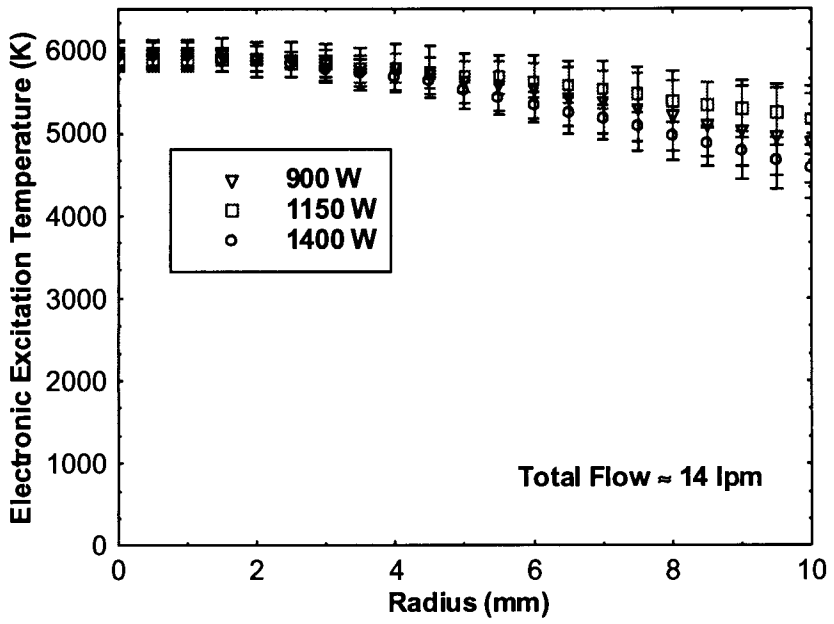

Figure 4-7. Electronic excitation temperature at constant flow for different microwave forward power levels.

Figure 4-8 displays the results of this study for a representative Fe I transition. The localized light emission profiles have been normalized to the same value on axis. The plasma diameter decreases slightly as the total airflow rate increases. For a total airflow rate increase of 11 lpm to 28 lpm the plasma radius at FWHM decreases from 7.0 to 6.0 mm corresponding to a cross-sectional area or plasma volume decrease inside the waveguide of 27 %. This result suggests an improved confinement of the plasma by increasing the total airflow rate.

The electronic excitation temperature is again obtained by utilizing the localized plasma light emission intensities of 12 or more Fe I transitions like the one shown in Figure 4-8. The resulting T_{exc} profiles for the various airflows are plotted in Figure 4-9. The temperature profiles are again almost flat, but now an increase in temperature is observed as the airflow increases. The axial temperature increases 13 % from 5800 K ± 200 K to 6550 K ± 350 K over the range of airflow studied. For the highest airflow at 28 lpm the temperature data is possible only out to an 8 mm radius because of the decrease in the plasma light emission diameter. The temperature profile at the highest flow also looks much flatter.

The observed temperature increase with airflow is contrary to expectations. Increasing the flow velocity through the plasma is expected to cool the plasma and reduce temperatures. Ogura *et al.* [6] report the lowest electronic excitation values with the highest carrier gas flow rate. This decrease is attributed to an increased plasma loading of particulates and a reduced plasma residence time. In the present MPT case increasing the axial flow rate does not correspondingly increase the feed rate and apparently a decreased residence time does not reduce the plasma temperature within the range of flow velocities of the present experiment.

4.6 Discussion

4.6.1 Interpretation of T_{exc} Profiles

The lack of dependence of T_{exc} on the microwave power can be understood in terms of the high collisionality of atmospheric pressure plasmas. The atmospheric microwave plasma is weakly ionized even for the highest electron density torch plasmas. The dominant electron collisions are with neutrals. As given in Timofeev [21] this collision frequency can be estimated by $\nu(T) = n(T)\, v_e(T)\sigma$, where $n(T) = n_o T_o / T$ is the neutrals density, n_o is the Loschmidt number (2.69 x 10^{19} cm^{-3}), T_o is room temperature, $v_e(T) = \sqrt{3kT/m_e}$, and σ is the cross-section for electron-neutral collisions which is assumed to be 10^{-15} cm^2. For the measured MPT temperature of 5800 K the electron-neutral collision frequency is thus estimated as 7 x 10^{10} s^{-1}. During one 2.45 GHz microwave cycle, an electron experiences more than 25 collisions with a mean free path between collisions of about 7 μm. The microwave electric field has insufficient time to accelerate the electrons to a high energy before inelastic collisions with neutrals cause the electrons to lose energy.

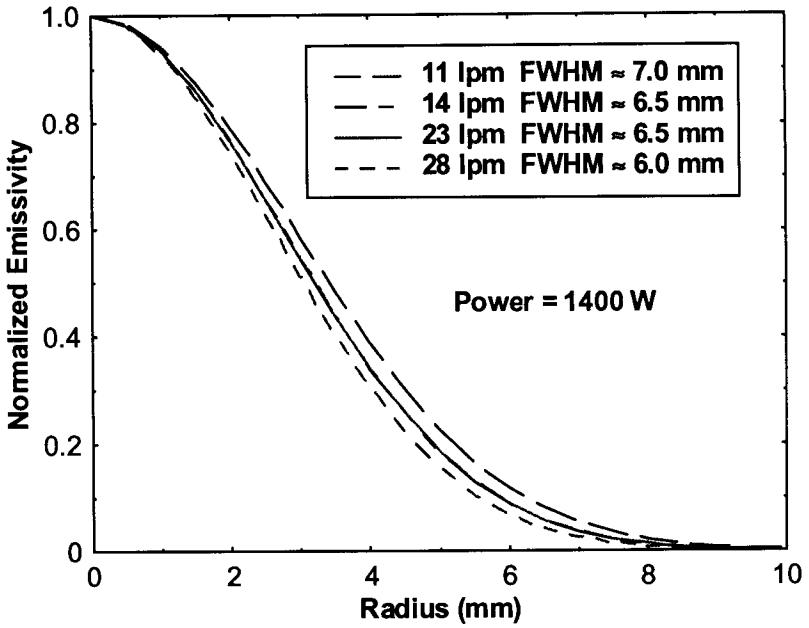

Figure 4-8. Normalized light emission at constant power with varying flow rate for a representative Fe I transition.

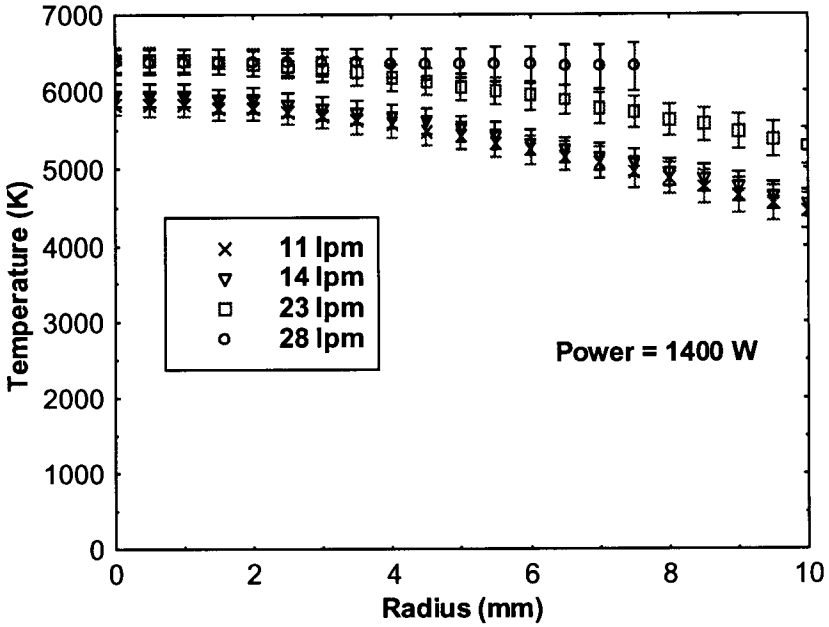

Figure 4-9. Electronic excitation temperature at constant microwave power for different total gas flow rates.

The internal energy states in an air plasma matrix limit the electron temperature through the high collision rate. However, all the microwave energy is absorbed as the forward power is increased. The measurements show that at a constant airflow rate this added energy goes to increasing the plasma volume rather than increasing the temperature. This fact is not a detriment for a MPT air metals pollution monitor. Estimates show that the sample species in the axial flow diffuses away from the center of the plasma as the gas flows through the waveguide [24]. The expansion of the plasma diameter at high microwave power ensures an enlarged region in which the species may experience excitation. If the plasma is optically thin, which is the case for most metals of interest, the extra light emission can be collected to increase detection limits. This technique is in fact utilized when the MPT is viewed axially rather than radially to increase the light collection path length in the plasma to obtain lower detection limits [7].

Unfortunately, not all atomic emissions are optically thin in an atmospheric plasma and therefore a larger plasma does not help. In the important case of mercury the strongest transitions terminate on the ground state. Consequently, the unexcited atoms cause self-absorption [11]. In this case the excitation efficiency must be increased to the lower detection limits, which requires more electrons with energies above the 4.9 eV excitation energy for mercury.

The measurements show that higher plasma temperatures are possible with higher airflow rates that cause the plasma to become more constricted. In Figure 6, the plasma volume decreases by ~27% as the gas flow rate increases from 11 lpm to 28 lpm. The peak temperature on axis correspondingly increases by ~13% as shown in Figure 4-9. This improved plasma confinement may, in part, be attributed to a high swirl flow rate in the 28 lpm total gas flow rate regime. The microwave energy absorbed does not change and thus with the smaller plasma volume the temperature rises. Therefore, for improving MPT performance for monitoring applications of some metals such as mercury, this result suggests that engineering smaller constricted microwave plasmas of high power could produce higher temperature for more efficient atomic excitation.

4.6.2 Skin Depth

The plasma cross-section size that can be driven efficiently by microwaves will be determined by what the absorption depth or skin depth is in the plasma. The results presented here demonstrate that the skin depth for the present MPT must be of the order of the plasma radius. If it were much more there would be large reflected power. If it were less the emissivity profiles in these figures would display a flattening or hollowing near the center of the plasma as observed in ICP plasmas with skin depths less than the plasma radius [25]. Therefore, the skin depth for the MPT must be about 0.5 cm for single pass absorption to be efficient.

Lieberman and Lichtenberg [26] describe the collisional skin depth, δ, by

$$\delta = \frac{\sqrt{2}c}{\omega_{pe}}\left(\frac{\nu}{\omega}\right)^{\frac{1}{2}} \tag{4-8}$$

where c is the speed of light in a vacuum, $\omega_{pe} = \sqrt{e^2 n_e / \varepsilon_o m_e}$ is the electron plasma frequency in radians s^{-1}, ν is the momentum collision frequency in Hz, and ω is the microwave frequency in radians s^{-1}. Equation 4-8 is valid only if ω_{pe}, $\nu >> \omega$, which is true for the present MPT experiments.

Evaluation of Equation 4-8 requires knowledge of the electron density, which was not measure. However, this equation can be rearranged to solve for the electron density using the observed plasma radius as the skin depth and the collision frequency derived above. The resulting electron density is ~ 10^{13} cm^{-3}, which is consistent with the MPT measurements of Ogura et al [6]. This result suggests that the formalism of Equation 4-8 can be used to understand MPT performance. The observed increase in plasma temperature and continued efficient microwave absorption in a smaller plasma size agree with this model. Because of the dependence of the collision frequency on temperature, the skin depth will decrease as the temperature increases allowing total absorption by smaller plasmas. The electron density will probably also increase with temperature to help this scaling. Thus efficient higher temperature microwave plasmas should be possible for application to mercury monitoring.

Large MPT plasma dimensions are also possible, which can be of value to many processing applications that require electrodeless plasma operation. Conventional wisdom states that scaling RF driven ICP torches to higher power and larger dimensions requires going to lower frequencies. This reasoning is based on the frequency scaling of the skin depth. However, the atmospheric MPT plasma cross-section compares favorably with lower frequency RF driven ICPs at comparable powers. In addition, the MPT has a much higher coupling efficiency of electromagnetic energy to the plasma. Therefore, the MPT may be a superior technology for applications where electrodeless plasma operation is important.

4.7 Conclusions

Electronic excitation temperature profile measurements in an atmospheric pressure air microwave plasma torch over a power range of 900 to 1400 W show that power has little effect on temperature with all other parameters such as airflow rate held constant. Over this power range, T_{exc} remains constant at 5800 ± 200 K on axis with an almost flat temperature profile. The temperature decreases by less than 20% out to a radius of 10 mm where the plasma light emission has decreased by more 95% of the on axis intensity. Increasing power only causes the plasma diameter to become larger, leading to an increase in the plasma volume by about 100% over the studied power range.

The electronic excitation temperature does increase when the plasma column is confined to a smaller diameter by increased axial and swirl airflow. Increasing the total airflow

from 11 to 28 lpm reduces the plasma volume by about 25 % and increases the electronic excitation temperature by about 13 % to 6550 ± 350 K. The continued efficient absorption of all the microwave power with smaller plasma cross-section is consistent with a collisional skin depth model when temperature also increases. The efficient atmospheric microwave plasma torch should find useful applications where electrodeless and high throughput operations are important.

4.8 References

[1] A. T. Zander and G. M. Hieftje, "Microwave-supported discharges", *Applied Spectroscopy* vol. 35, no.4, pp. 357 –371, 1981.

[2] K. Fallgatter, V. Svoboda, and J. D. Winefordner, "Physical and analytical aspects of a microwave excited plasma", *Applied Spectroscopy*, vol. 25, no. 3, pp. 347 –352, 1971.

[3] K. A. Forbes, E. E. Reszke, P. C. Uden, and R. M. Barnes, "Comparison of microwave-induced plasma sources", *J. of Analytical Atomic Spectrometry*, vol. 6, pp. 57 –71, February 1991.

[4] K. C. Ng and W .L. Shen, "Solution nebulization into low-power argon microwave-induced plasma for atomic emission spectrometry: study of synthetic ocean water", *Anal. Chem*, vol. 58, pp. 2084 –2087, 1986.

[5] Y. Okamoto, "Annular-shaped microwave-induced nitrogen plasma at atmospheric pressure for emission spectrometry of solutions", *Analytical Sciences*, vol. 7, pp. 283 –288, April 1991.

[6] K. Ogura, H.Yamada, Y Sato, and Y. Okamoto, Excitation temperature in high-power nitrogen microwave-induced plasma at atmospheric pressure", *Applied Spectroscopy*, vol. 51, no. 10 pp. 1496 –1499, 1997.

[7] P. P. Woskov, K. Hadidi, P. Thomas, K. Green, and G. Flores, "Accurate and sensitive metals emissions monitoring with an atmospheric microwave-plasma having an real-time span calibration", *Waste Management*, vol. 20, pp. 395-403, 2000.

[8] H. Potts and J. Hugill, "Studies of high-pressure, partially ionized plasma generated by 2.45 GHz, microwaves", *Plasma Sources Sci. Technol., vol. 9, pp. 18-24, 2000.*

[9] J. E. Brandenburg and J. F. Kline, "Experimental Investigation of Large-Volume PIA Plasmas at Atmospheric Pressure", *IEEE Trans. on Plasma Sci.*, vol. 26, no. 2, pp. 145-149, 1998.

[10] K. Hadidi, P. P. Woskov, G. J. Flores, K. Green, and P. Thomas, "Effect of oxygen concentration on the detection of mercury in an atmospheric microwave discharge", *Jpn. J. Appl. Phys.*, vol. 38, pp. 4595-4600, 1999.

[11] K. Hadidi, P. P. Woskov, K. Green, and P. Thomas, "Observation of self absorption of mercury I and cadmium I emission in an atmospheric microwave sustained plasma", *J. Anal. At. Spectrom.*, vol. 15, pp. 601-605, 2000.

[12] A. M. Gomes, J. Bacri, J. P. Sarrette, and J. Salon, "Measurement of heavy particle temperature in a radiofrequency air discharge at atmospheric pressure from the numerical simulation of the NOγ system" *Journal of Analytical Atomic Spectrometry*, vol. 7 pp. 1103 –1109, October 1992.

[13] M. H. Abdallah and J. M. Mermet, "The behavior of nitrogen excited in an inductively coupled argon plasma", *J. Quant. Spectrosc. Radiat. Transfer*, vol. 19, pp. 83 –91, 1978.

[14] G. J. Flores, "Establishing a calibration for a microwave plasma continuous emissions monitor", Master 's Thesis, Massachusetts Institute of Technology, Nuclear Engineering Department, 1998.

[15] P. W. J. M. Boumans, editor, *Chemical Analysis*, vol. 90, John Wiley & Sons, Inc., New York, Chapters 10-11, 1987.

[16] K. Miyamoto, *Plasma Physics for Nuclear Fusion*, The MIT Press, Cambridge, Massachusetts, revised edition, 1989.

[17] I.H.Hutchinson, Principles of Plasma Diagnostics, Cambridge University Press, Cambridge, 1994.

[18] J. P. Matousek, B. J. Orr, and M. Selby, "Microwave-induced plasmas: Implementation and application", *Prog. analyt. atom. Spectrosc.*, vol. 7, pp. 275 – 314, 1984.

[19] J. F. Alder, R. M. Bombelk, and G. F. Kirkbright, "Electronic excitation and ionization temperature measurements in a high frequency inductively coupled argon plasma source and the influence of water vapor on plasma parameters", *Spectrochimica Acta B*, vol. 35, pp.163 –175, 1980.

[20] H. R. Griem, *Plasma Spectroscopy*, McGraw-Hill Book Company, New York, 1964.

[21] A. V. Timofeev, "Theory of microwave discharges at atmospheric pressures", *Plasma Physics Reports*, vol. 23, no. 72, pp. 158 –164, 1997.

[22] M. C. Borrás, K. Hadidi, P. Woskov, K. M. Green, G. J. Flores, and P. Thomas, "An experiment for radial temperature profile measurements in a microwave induced plasma at atmospheric pressure", IEEE Conference Record-Abstracts, p. 169, 1998 IEEE International Conference on Plasma Science, Raleigh, NC, June 1-4, 1998.

[23] M. H. Abdallah, and J. M. Mermet, "Comparison of temperature measurements in ICP and MIP with Ar and He as plasma gas", *Spectrochimica Acta B* , vol. 37, no. 5, pp. 391 –397, 1982.

[24] B. R. Pollack, "Establishing isokinetic flow for a plasma torch exhaust gas diagnostic for a plasma hearth furnace", Master 's Thesis, Massachusetts Institute of Technology, Nuclear Engineering Department and Mechanical Engineering Department, 1996.

[25] M. I. Boulos, "The inductively coupled RF (radio frequency) plasma", *Pure & Appl. Chem.*, vol. 57, no. 9, pp. 1321-1352, 1985.

[26] M. A. Lieberman and A. J. Lichtenberg, *Principles of Plasma Discharges and Materials Processing*, John Wiley & Sons, Inc., New York, 1994.